SANDIA REPORT

SAND2014X-XXXX

Unlimited Release

Printed September 2014

Modeling and Validation of the Thermal Response of TDI Encapsulating Foam as a function of Initial Density

Marvin E. Larsen and Amanda B. Dodd

Prepared by
Sandia National Laboratories
Albuquerque, New Mexico 87185 and Livermore, California 94550

Sandia National Laboratories is a multi-program laboratory managed and operated by Sandia Corporation, a wholly owned subsidiary of Lockheed Martin Corporation, for the U.S. Department of Energy's National Nuclear Security Administration under contract DE-AC04-94AL85000.

Issued by Sandia National Laboratories, operated for the United States Department of Energy by Sandia Corporation.

Available to DOE and DOE contractors from
U.S. Department of Energy
Office of Scientific and Technical Information
P.O. Box 62
Oak Ridge, TN 37831

Telephone: (865) 576-8401
Facsimile: (865) 576-5728
E-Mail: reports@adonis.osti.gov
Online ordering: http://www.osti.gov/bridge

Available to the public from
U.S. Department of Commerce
National Technical Information Service
5285 Port Royal Rd.
Springfield, VA 22161

Telephone: (800) 553-6847
Facsimile: (703) 605-6900
E-Mail: orders@ntis.fedworld.gov
Online order: http://www.ntis.gov/help/ordermethods.asp?loc=7-4-0#online

ABSTRACT

TDI foams of nominal density from 10 to 45 pound per cubic foot were decomposed within a heated stainless steel container. The pressure in the container and temperatures measured by thermocouples were recorded with each test proceeding to an allowed maximum pressure before venting. Two replicate tests for each of four densities and two orientations in gravity produced very consistent pressure histories. Some thermal responses demonstrate random sudden temperature increases due to decomposition product movement. The pressurization of the container due to the generation of gaseous products is more rapid for denser foams. When heating in the inverted orientation, where gravity is in the opposite direction of the applied heat flux, the liquefied decomposition products move towards the heated plate and the pressure rises more rapidly than in the upright configuration. This effect is present at all the densities tested but becomes more pronounced as density of the foam is decreased.

A thermochemical material model implemented in a transient conduction model solved with the finite element method was compared to the test data. The expected uncertainty of the model was estimated using the mean value method and importance factors for the uncertain parameters were estimated. The model that was assessed does not consider the effect of liquefaction or movement of gases. The result of the comparison is that the model uncertainty estimates do not account for the variation in orientation (no gravitational affects are in the model) and therefore the pressure predictions are not distinguishable due to orientation.

Temperature predictions were generally in good agreement with the experimental data. Predictions for response locations on the outside of the can benefit from reliable estimates associated with conduction in the metal. For the lighter foams, temperatures measured on the embedded component fall well with the estimated uncertainty intervals indicating the energy transport rate through the decomposed region appears to be accurately estimated. The denser foam tests were terminated at maximum allowed pressure earlier resulting in only small responses at the component. For all densities the following statements are valid: The temperature response of the embedded component in the container depends on the effective conductivity of the foam which attempts to model energy transport through the decomposed foam and on the stainless steel specific heat. The pressure response depends on the activation energy of the reactions and the density of the foam and the foam specific heat and effective conductivity. The temperature responses of other container locations depend heavily on the boundary conditions and the stainless steel conductivity and specific heat.

LIST OF FIGURES

LIST OF TABLES

1. INTRODUCTION

This report describes the results of a series of experiments characterizing the thermal response of TDI (toluene diisocyanate) –polyester-polyol polyurethane foam contained in a heated can. The test set provides the means to provide a well-controlled boundary condition simulating fire conditions resulting the in thermal decomposition of encapsulant foam in a metal container. The basic test apparatus has been used in several other studies [1-3]. This study analyzes tests focused on characterizing the effect of initial foam density on the system thermal and pressurization responses for TDI foam. This set of experiments was conducted in 2010.

The following section (2) describes the test apparatus and important parameters of the tests. Four nominal foam densities ranging from 10 to 45 lb/ft^3 were targeted. Each of four densities were tested twice in upright and inverted orientations resulting 16 experiments.

Prior to describing any modeling effort, Section 3 is devoted to presenting the measured temperature and pressure responses. Some dependence upon the initial foam density is evident but thermal conduction in the can, constant across the test series, also plays a significant role in the overall response.

The chemistry and transport model details have been previously described [1-3]. The model equations are solved using Aria, the finite element thermal analysis code in the SIERRA toolbox. Additional model development has occurred in improving the representation of the heated boundary. These details are included in Section 4.

Section 6 describes the mean value method as implemented to perform uncertainty quantification (UQ). Section 7 describes the parameters identified for use in the UQ Assessment.

Section 8 presents results of the UQ assessment.

Finally, conclusions are presented in Section 9.

2. EXPERIMENTAL SETUP

References [1-3] include detailed descriptions of the experimental set-up and foam-in-can test article which are shown in Figure 1 and Figure 2. The outside dimensions of the foam can are 3.25 in. (83 mm) high by 3.5 in. (89 mm) in diameter. The 0.020 in. (0.5 mm)-wall-thickness sleeve is joined to a lid of 0.375 in. (8.8 mm) thickness and the "component" by electron beam welding. The can interior was filled with TDI foam of nominal 10, 20, 30, and 45 lb/ft^3 density. Table 1 summarizes the actual densities realized for the tests. The rms foam density deviation from the nominal target densities is 3.3% for the sixteen tests, with the biggest error being associated with TDI20-4.

As shown in Figure 2 there are four thermocouples (TC1-TC4) in the heated lid, four in the base (TC13 – TC16), three down each side under the vent tubes (TC5-TC7 and TC9-TC11), and three near the face of the component (TC17, TC18, TC20). The model discussed later has a coordinate frame such that positive X, Y, and Z are into Figure 2, downward, and right-to-left. In that frame TC1 and TC3 are on a line parallel to the X-axis and the same distances from the center of the lid as TC2 and TC4. TC13 and TC15 are likewise positioned in the bottom end.

Table 1: Summary of experiments and actual foam densities.

Test Designator	Orientation	Foam Mass (grams)	Foam Density (lb/ft^3)	Foam Density (kg/m^3)	% Dev. from Nominal
TDI10-1	U1	33.43	10.07	161.3	0.7
TDI10-2	U2	33.04	9.948	159.4	-0.5
TDI10-3	I1	34.35	10.34	165.7	3.4
TDI10-4	I2	33.37	10.05	161.0	0.5
TDI20-1	U1	65.73	19.79	317.1	-1.1
TDI20-2	U2	65.95	19.86	318.2	-0.7
TDI20-3	I1	66.48	20.02	320.8	0.1
TDI20-4	I2	61.68	18.57	297.6	-7.1
TDI30-1	U1	96.49	29.05	465.6	-3.2
TDI30-2	U2	96.16	28.95	464.0	-3.5
TDI30-3	I1	95.63	28.79	461.4	-4.0
TDI30-4	I2	95.31	28.70	459.9	-4.3
TDI45-1	U1	143.2	43.11	690.9	-4.2
TDI45-2	U2	144.4	43.46	696.5	-3.4
TDI45-3	I1	144.3	43.45	696.3	-3.4
TDI45-4	I2	143.4	43.18	692.0	-4.0

Photos of experimental setups typical of the upright and inverted orientations of the stainless steel can are shown in Figure 1 and the present analysis considers two experiments conducted in each of those orientations for each of the four densities. The test orientations for a given density are referred to as “U1” or “Upright 1”, “U2” or “Upright 2”, “I1” or “Inverted 1”, and “I2” or “Inverted 2.” As indicated in the left column of Table 1, the tests are referenced in the foregoing order so that TDI10-1, TDI20-1, etc. are unique references for each test. In all of the experiments, temperature was monitored by a thermocouple (TC2 in Figure 2) in the heated lid and used to control lamp power to achieve a nominal heating rate of 200 K per minute to a maximum temperature of 1173 K (900°C) which is held until the end of the experiment. Pressure was also monitored at a vent tube and each experiment was ended upon reaching an internal can pressure of 2.5 MPa (350 psi), at which point a solenoid valve was opened to vent the pressure and the power to the heating lamps was interrupted.

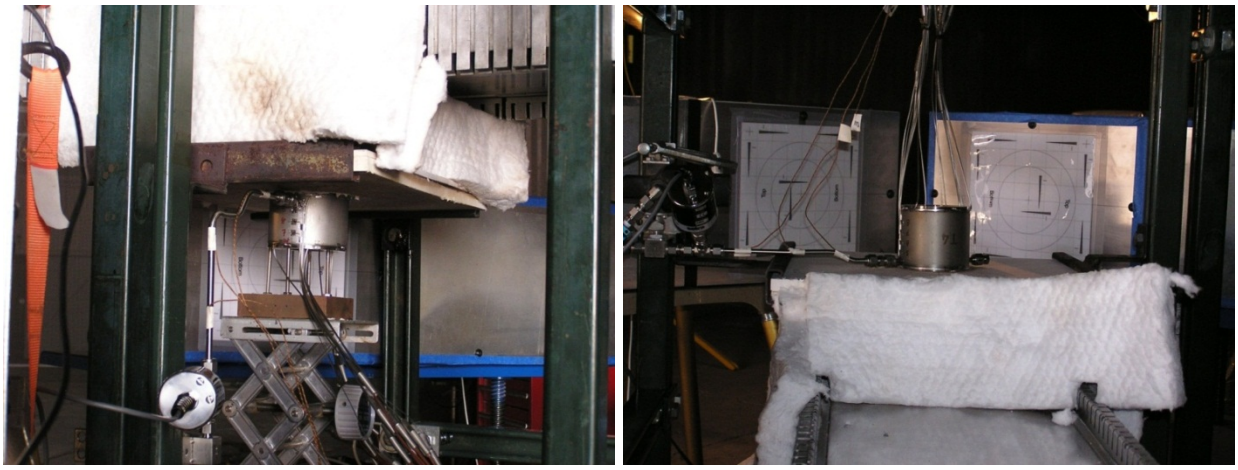

Figure 1: Typical experimental setups: left view is upright and right view is inverted.

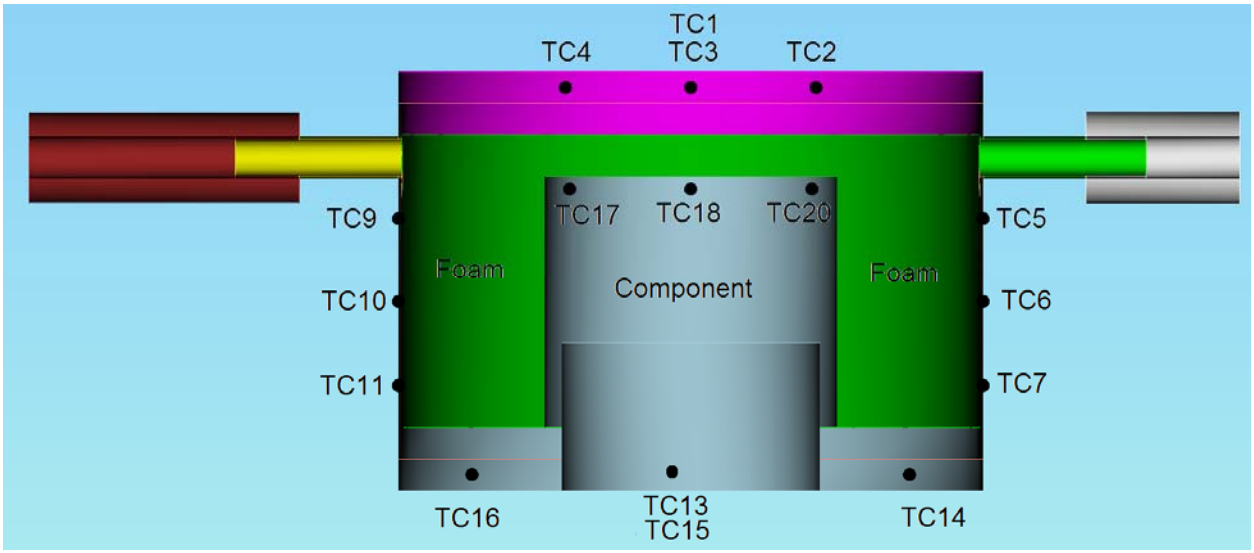

Figure 2: Thermocouple locations.

One vent tube was blocked with a plug fitting. The other tube was connected to a line to direct expelled decomposition products away from the experiment when the solenoid opened. In order to ensure that condensate from the products did not clog the discharge, the discharge line was heated with a tape heater prior to the onset of the experiment. This arrangement introduced some unknown asymmetry to the test article's initial temperature distribution. However, that temperature difference was small relative to the large temperature excursions promptly introduced by the experiment. Table 2 summarizes the differences seen in TC5 and TC9 and the beginning of each test normalized by the average temperature increase of the two locations for the test. The largest temperature difference (associated with TDI30-U2) of 20°C is about 7% of the excursion temperature excursion realized by TC5 and TC9 over the test. For that same test

TC10 and TC11 are 9.9 and 15.4°C less than TC9 demonstrating that the hot spot on the side of the can due to the tube heating is small.[1]

Table 2: Summary of initial TC5/TC9 temperature differences.

Nom. Density	Test	Initial δT (°C) $T_9 - T_5$	Average Max Temp (°C) $(T_{9,max} + T_{5,max})/2$	Average Min Temp (°C) $(T_{9,min} + T_{5,min})/2$	$\delta T/\Delta T$ (%)
10	U1	16.9	482.375	36.525	3.8
10	U2	15.1	481.275	36.49	3.4
10	I1	15.0	373.945	31.01	4.4
10	I2	14.9	385.8	39.955	4.3
20	U1	15.5	448.37	38.355	3.8
20	U2	19.7	441.47	38.545	4.9
20	I1	17.3	352.88	35.705	5.4
20	I2	15.8	341.075	36.215	5.2
30	U1	16.0	269.08	34.67	6.8
30	U2	20.5	319.54	40.58	7.4
30	I1	11.6	222.67	34.55	6.1
30	I2	12.5	231.96	35.65	6.4
45	U1	7.9	184.03	28.585	5.1
45	U2	9.0	191.48	27.245	5.4
45	I1	16.5	207.05	31.75	9.4
45	I2	11.2	173.89	33.63	8.0

As noted, each test was ended at an approximate can pressure of 350 psig (2.5 MPa). Consequently, tests for the upright orientation are approximately 7 minutes long and those of the inverted orientation are just under 4 minutes. All of the thermocouples and the pressure were recorded at one-second intervals.

3. EXPERIMENTAL RESULTS

This section presents the recorded measurements for each location. Figure 3 and Figure 4 show the measured lid temperature and the pressure response for the sixteen tests.

Ideally, except for the variation in initial temperature, the Figure 3 results would all be coincident as the targeted temperature schedule was the same. The small spread in the realized temperature schedule shows the measurement/controller error in conducting the experiment. Not all of the TC2 traces make it to the 900°C plateau because the test ends upon reaching the

[1] The thermocouples are at ½-inch intervals. Across from TC9, TC10, TC11 (TC5, TC6, TC7) there is only about 1°C difference in the three thermocouples.

maximum pressure. At about 150s the spread in observed TC2 is 46°C. The variation in initial temperature is small relative to the temperature increases for the tests.

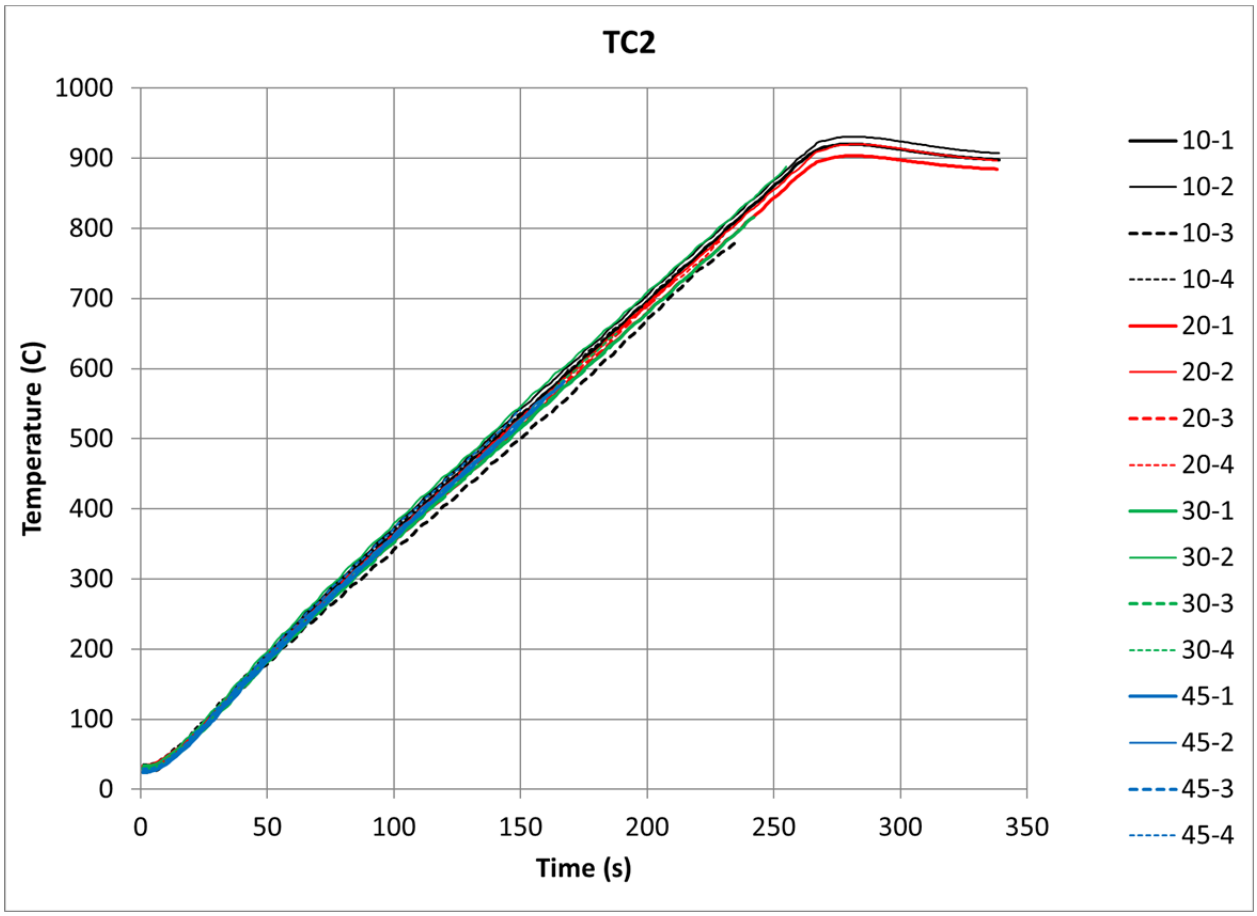

Figure 3: Thermocouple TC2 responses for all sixteen tests.

Figure 4 shows the pressure response for all sixteen tests. Lines of the same color are of a common nominal density and dashed lines represent the inverted geometries while solid lines represent upright orientation. It is clear that the pressure rises fastest for the test specimens with the highest initial density. For the less dense specimens, the dependence on orientation is clear. The replicate tests are remarkably consistent and in all cases, clearly showing similar general behavior. The inverted tests with 20lb/ft^3 foam show the greatest variability between the replicate tests. TDI20-4 arrives at 50 psig at approximately 159s whereas TDI20-3 reaches 50 psig 30s earlier. TDI20-4 (Table 1) initial foam density was less than intended so the trend between the two 20lb/ft^3 (inverted) tests is consistent with trend demonstrated for density. However, it appears that TDI20-4 is the outlier as the pressures from approximately 100s to 175s indicate lower pressures than were seen for the 10 lb/ft^3 inverted tests, which are very consistent with each other.

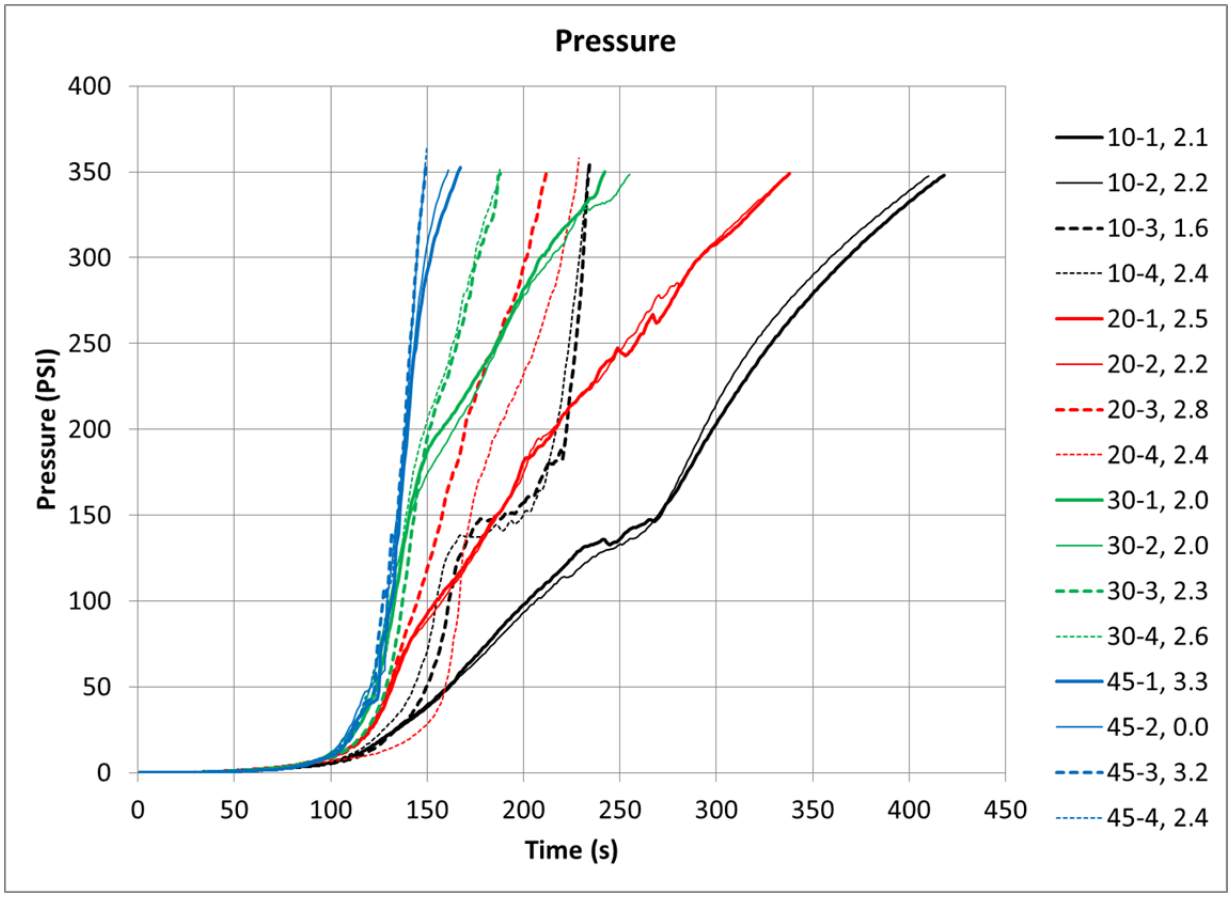

Figure 4: Measured pressure responses for all sixteen tests.

Figure 5 through Figure 20 show the measured responses at each of the locations for which data was recorded. In each case the common colors are for the same nominal density, dashed lines are for inverted geometry, and the first of each duplicate test is plotted with a heavier line. To facilitate response comparison, each measurement is presented as the increase in the measurement from the experiment zero time and legend entries present the initial value of the variable.

Figure 5 and Figure 6 show the TC2 and TC4 responses. These measurements are the lid's response and TC2 was used as the monitor for controlling heater input power. A little delay in the response relative to the straight-line ideal reflects the short interval of time for thermal diffusion from the lid surface to the controlling thermocouple. All cases are substantially on track. In the modeling effort to be reported later, these individual records of temperature history are used to define the system's boundary condition.

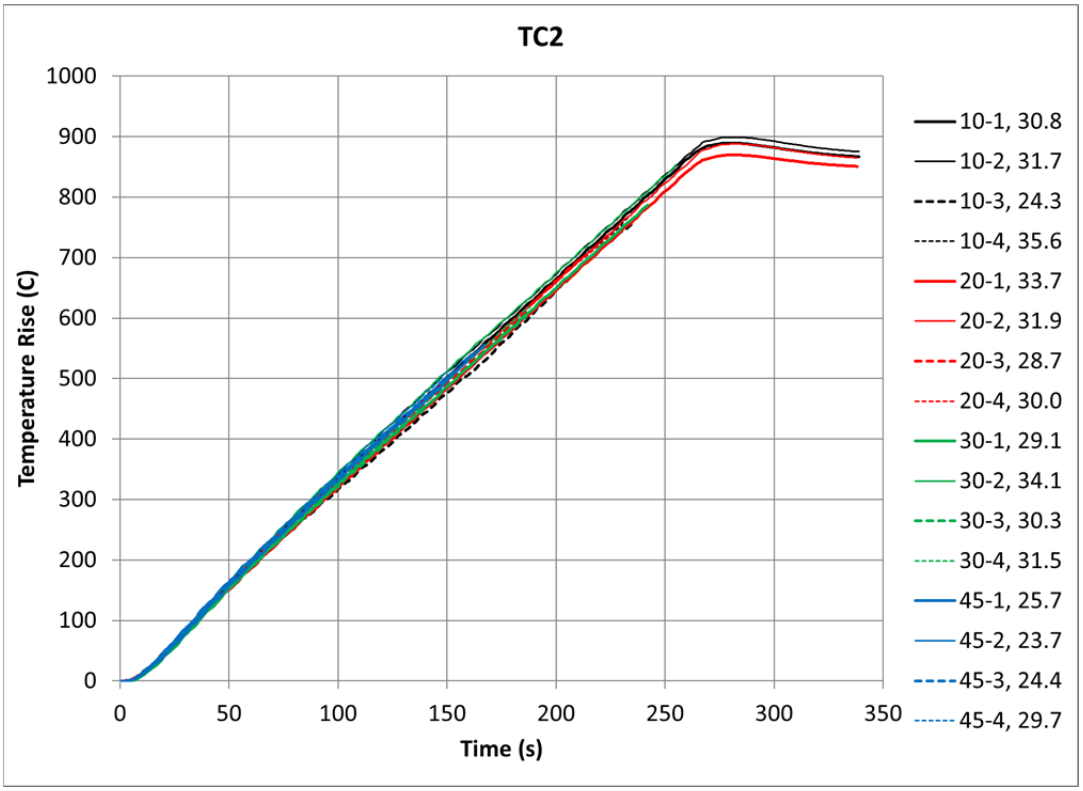

Figure 5: TC2 response for all tests.

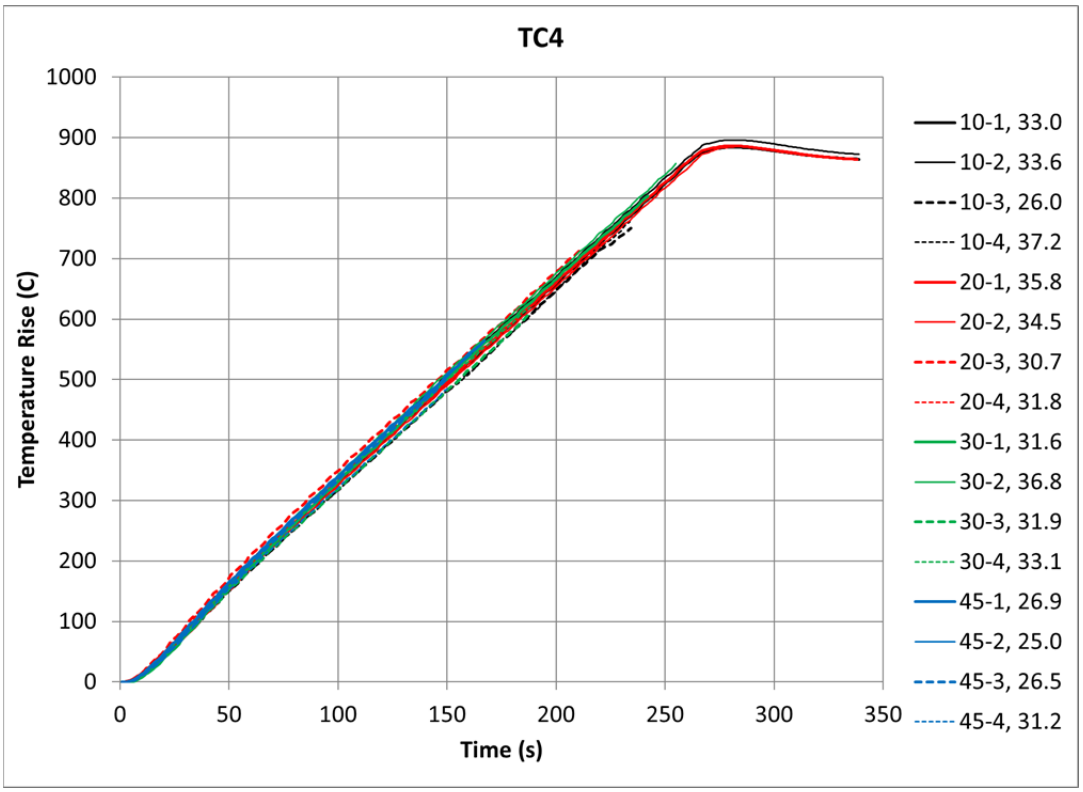

Figure 6: TC4 response for all tests.

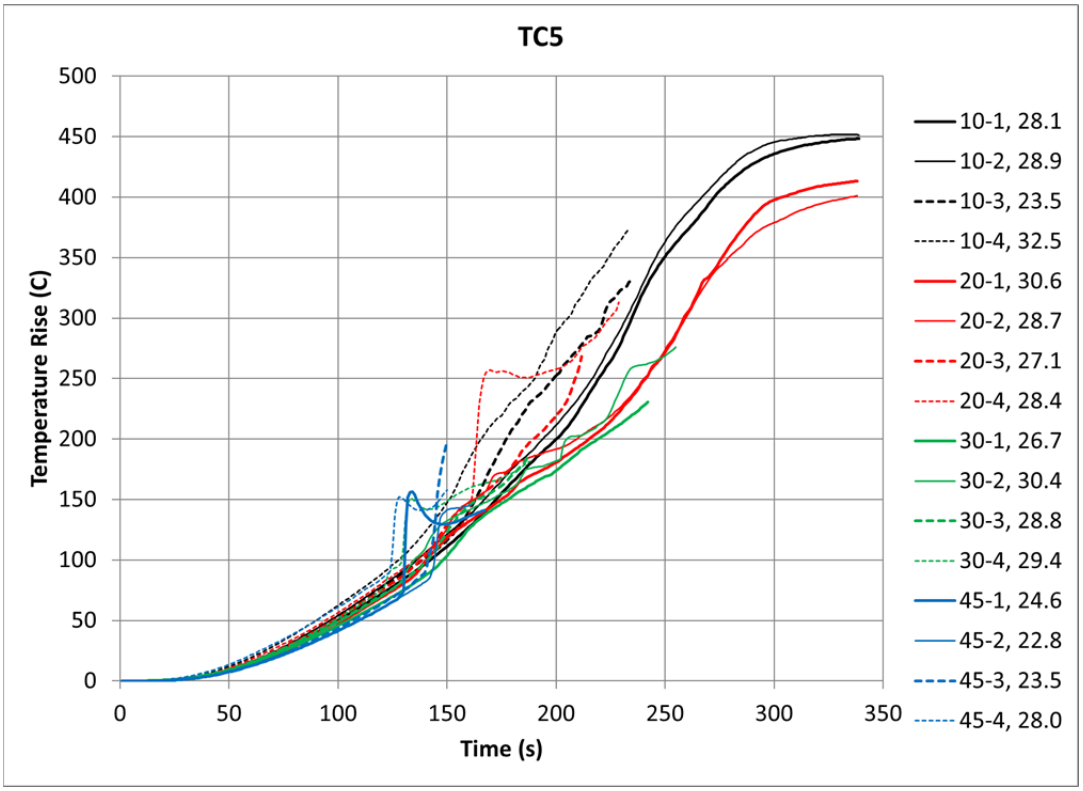

Figure 7: TC5 response for all tests.

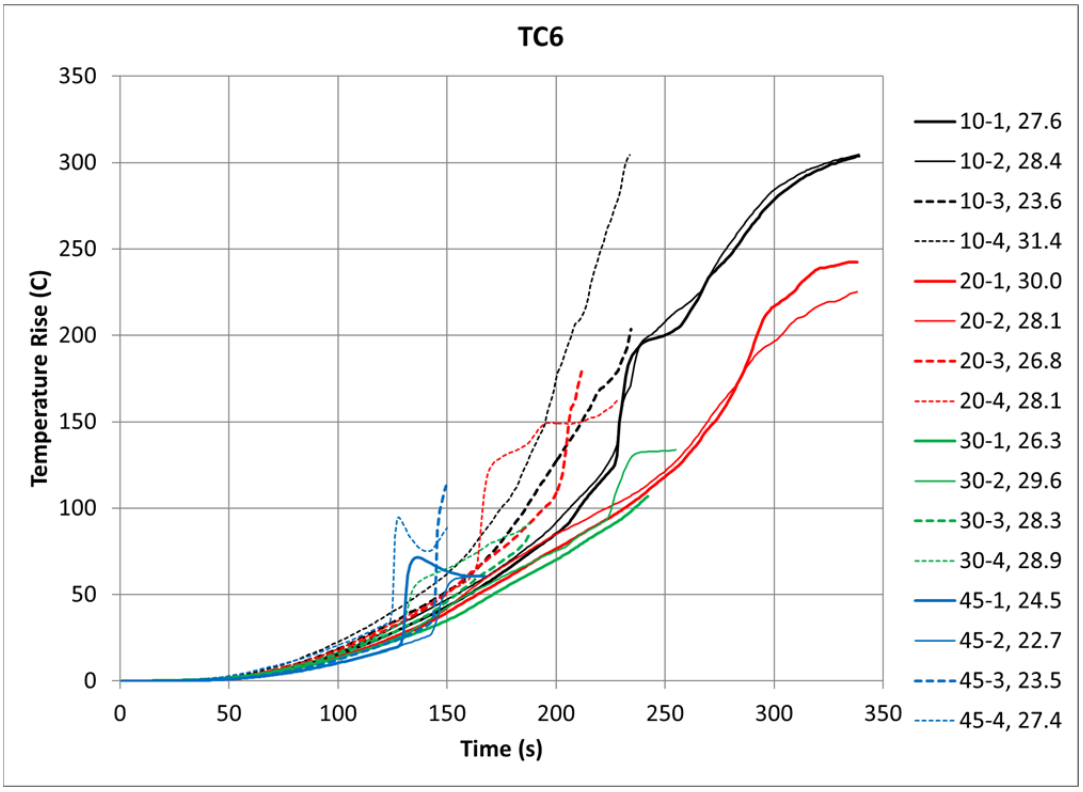

Figure 8: TC6 response for all tests.

Figure 7, Figure 8, and Figure 9 show the responses for thermocouples TC5, TC6, and TC7 which are at 0.5-inch intervals down one side of the can. An interesting feature in these plots are the sudden temperature rises that occur on some of the traces. All of the 45 lb/ft^3 foam tests show an event between about 125s and 150s in which the time rate of change $(\partial T/\partial t)$ suddenly changes. At approximately 125s, the temperatures TDI45-4 TC5, TC6, and TC7 all increase rapidly almost simultaneously. This is pretty clear evidence of hot decomposition products moving along the can edge. After the sharp increase in temperature, each of the locations cools down in a way consistent with local thermal diffusion. Similar events are seen on many of the transient temperature responses, occurring for either orientation and most prominently for the denser foams.

Figure 10, Figure 11, and Figure 12 plot the responses of TC9, TC10, and TC11 which are diametrically opposed from TC5, TC6, and TC7. Sudden temperature excursions similar to those of TC5, TC6, and TC7 are seen. In fact, the 30 lb/ft^3 and 45 lb/ft^3 tests show sudden excursions at the same times as those occurring across the can, perhaps due to gases moving down the sides of the can or through the foam.

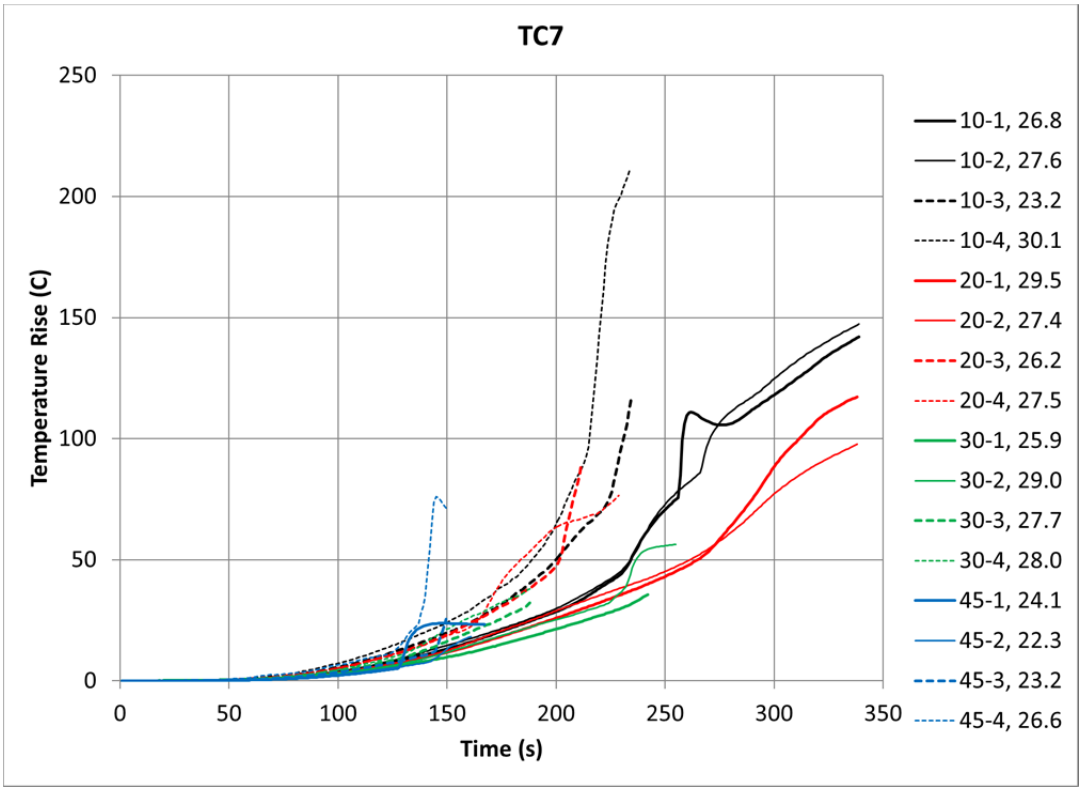

Figure 9: TC7 response for all tests.

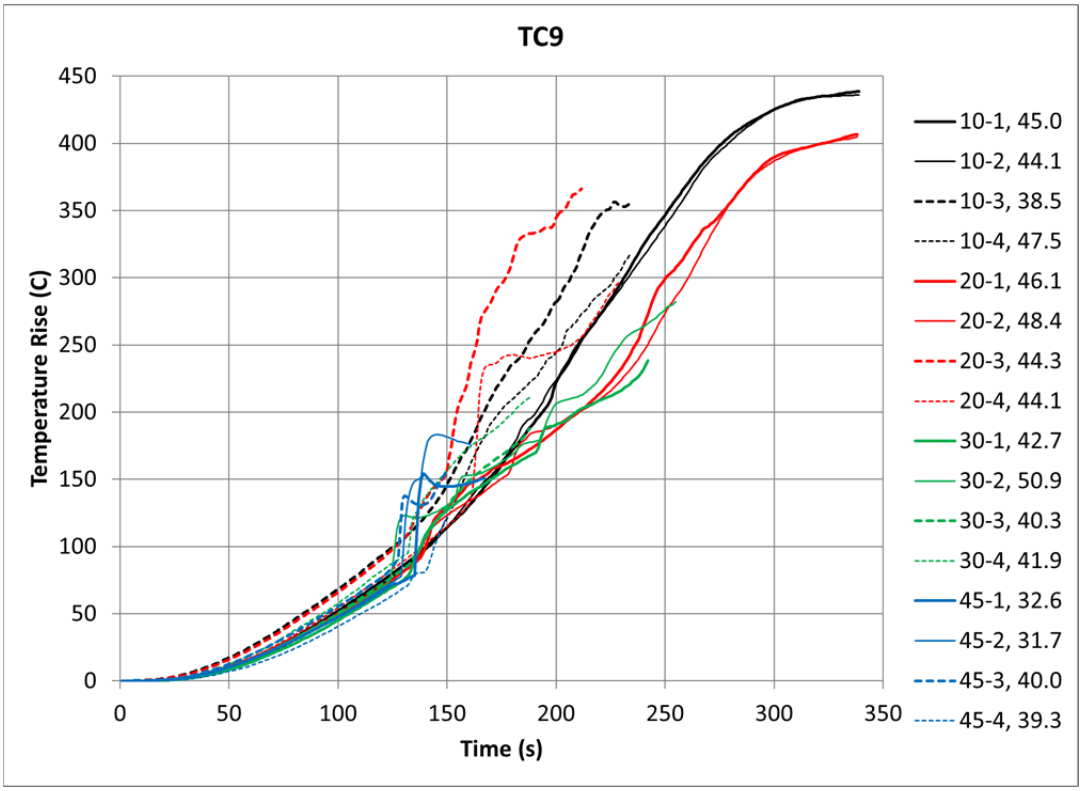

Figure 10: TC9 response for all tests.

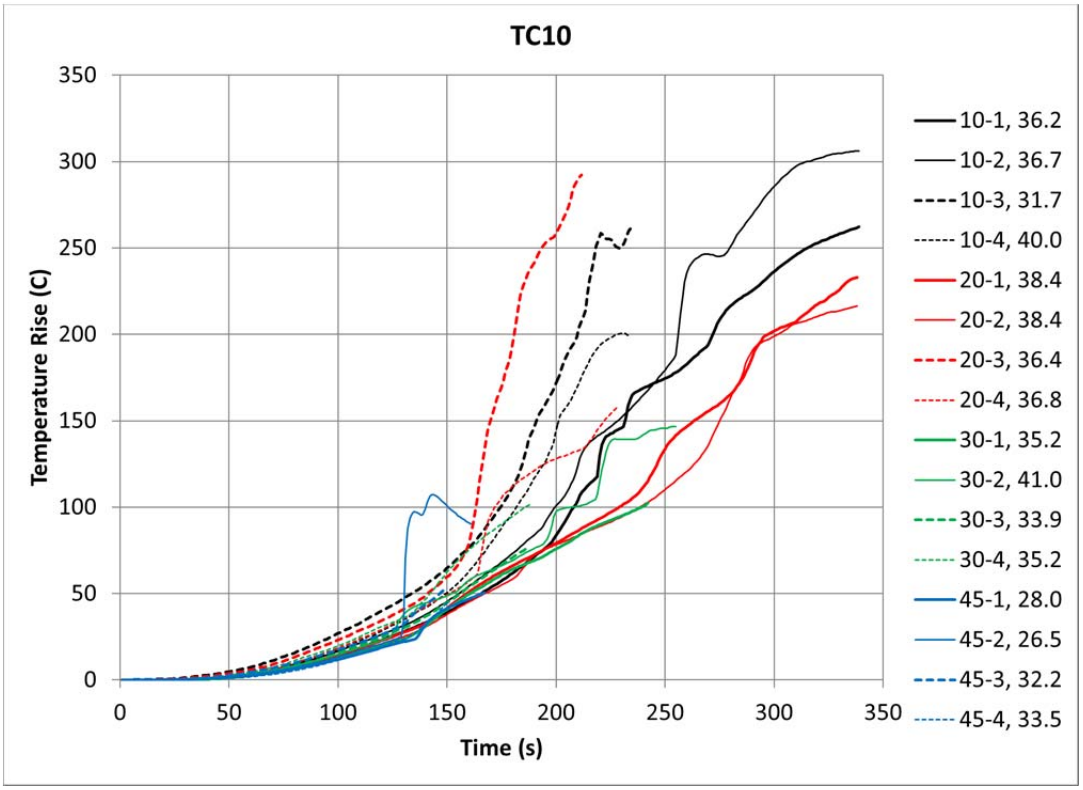

Figure 11: TC10 response for all tests.

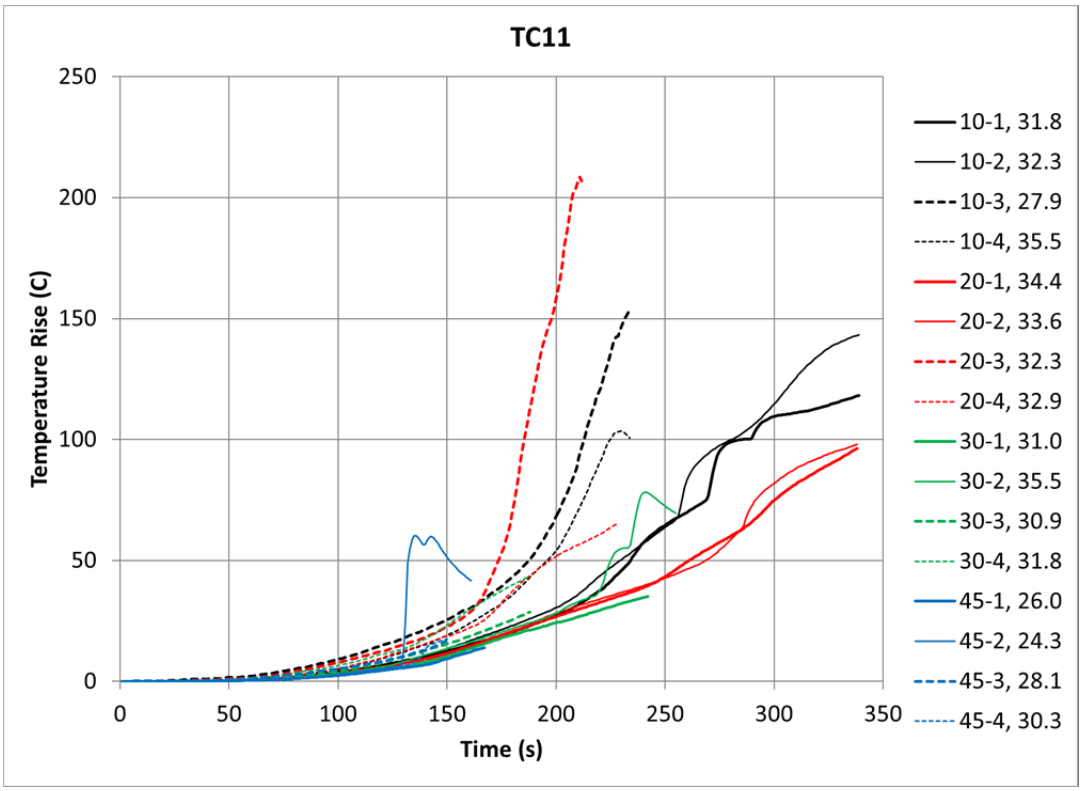

Figure 12: TC11 response for all tests.

Figure 13 through Figure 16 correspond to locations (TC13, TC14, TC15, TC16) near the periphery of the sealing lid ("bottom" of the can) opposite the heated lid. For the most part, prior to approximately 200s these responses all look like that associated with a thermal diffusion wave arriving from the distant heated boundary. After that time many of the responses turn up sharply. Note in Figure 14 the sudden rise in temperature for TDI45-4 at 140s. TC14 is on the same side of the can as TC5, TC6, and TC7. In Figure 9 there is a prominent sudden rise in TC7 for TDI45-4 it appears that that same event reaches the far extreme of the can. It is thought that due to the high density of the initially close cell foam, gaseous products might be moving along the sides and edges of the can, heating the exterior of the can as they move.

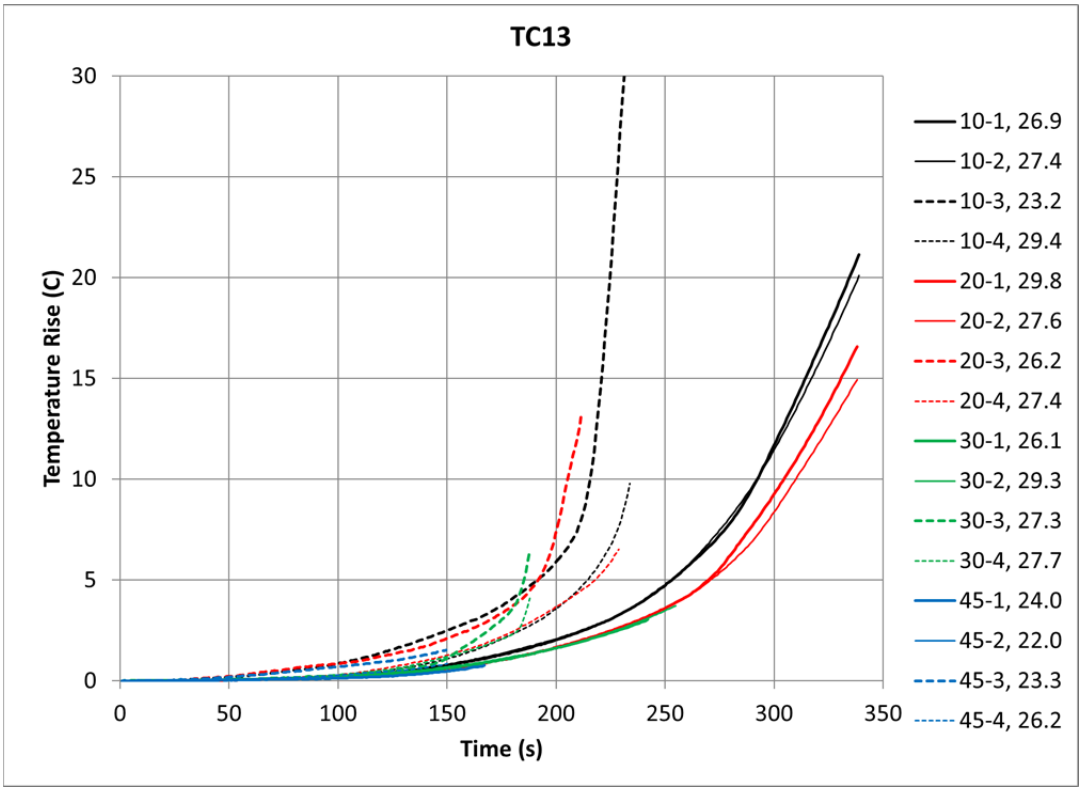

Figure 13: TC13 response for all tests.

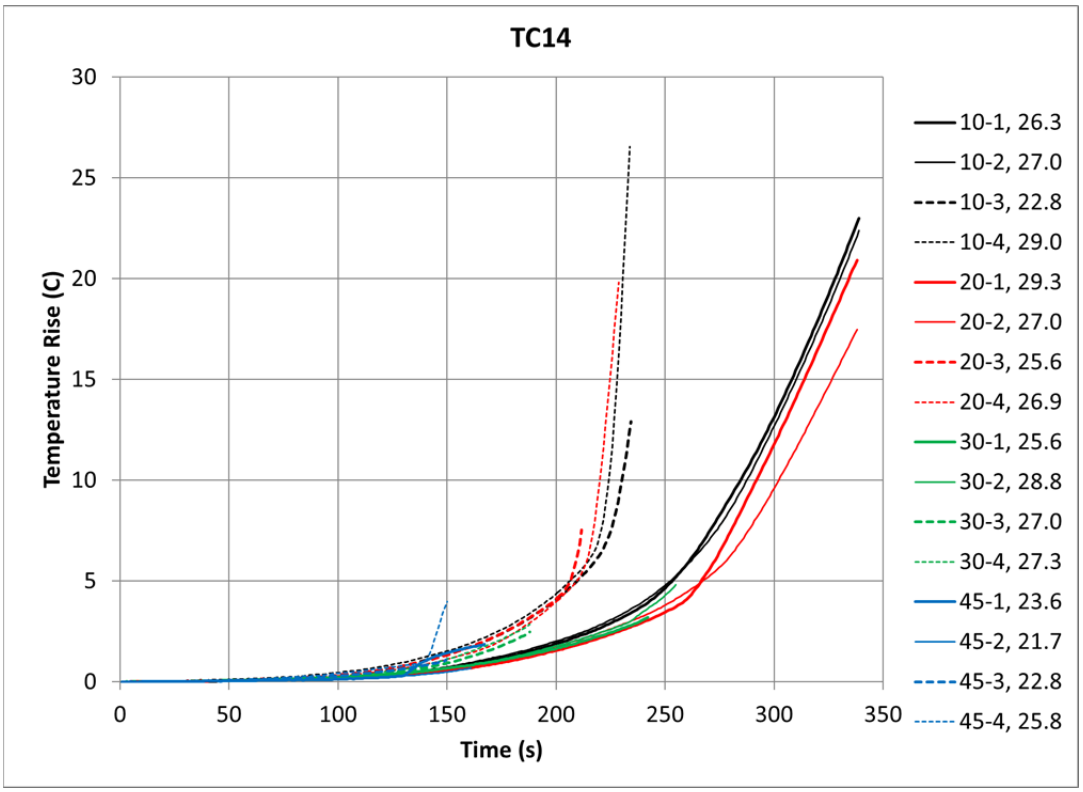

Figure 14: TC14 response for all tests.

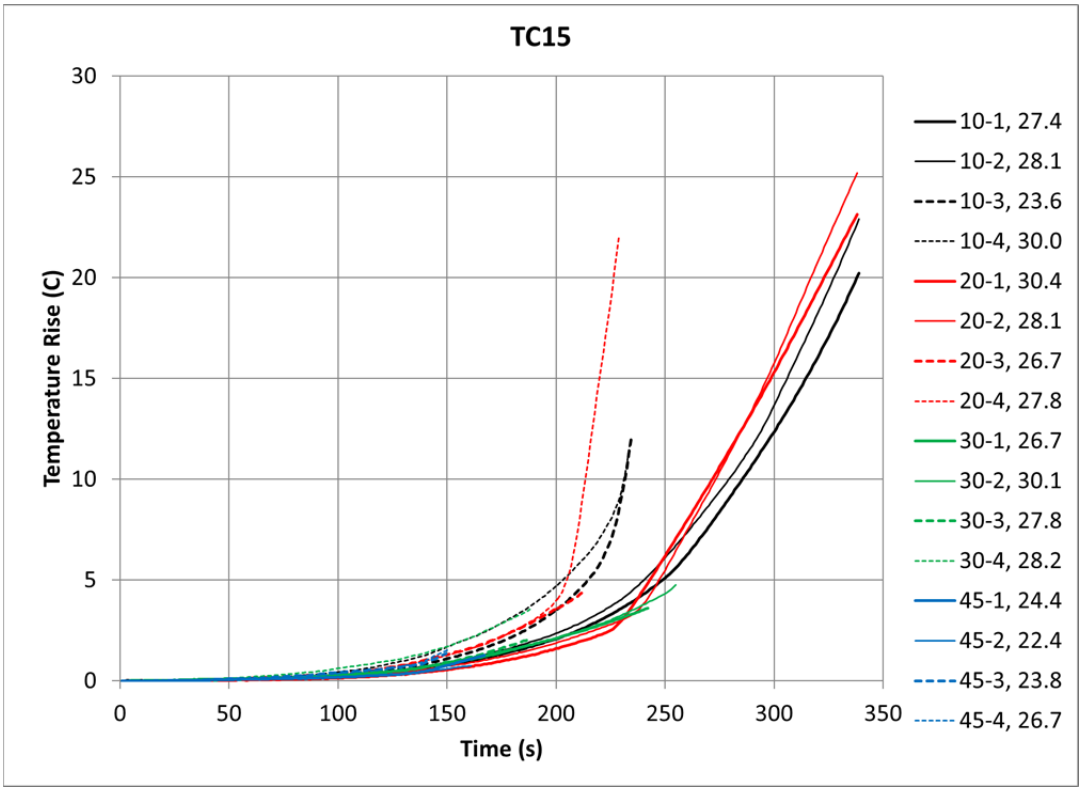

Figure 15: TC15 response for all tests.

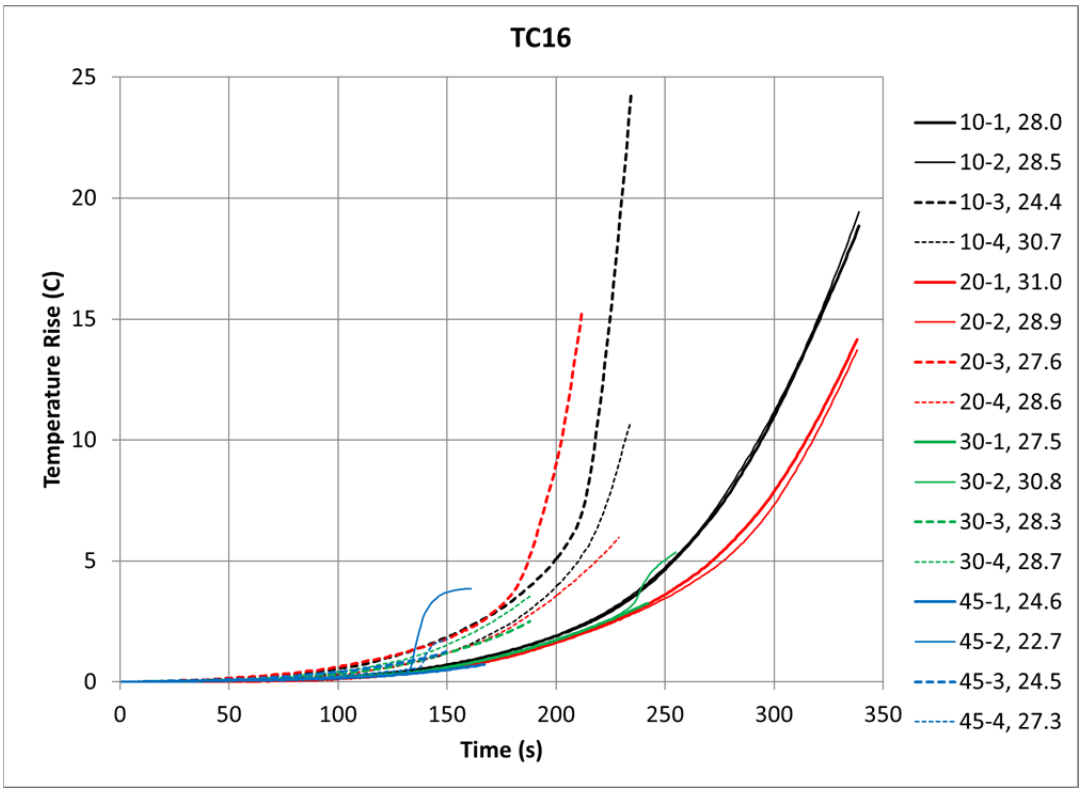

Figure 16: TC16 response for all tests.

Figure 17, Figure 18, and Figure 19 correspond to TC17, TC18, and TC20, which measure responses in the embedded component's face nearer the heated can surface. The cases of the longer running experiments, TDI10-1, TDI10-2, TDI20-1, and TDI20-2 show qualitatively similar late responses. By design, these locations are distant from the heated surface in terms of conduction paths through the metallic part of the system. Consequently, the late heating of the component is a fairly direct indication of the transport of energy across the gap of decomposed foam.

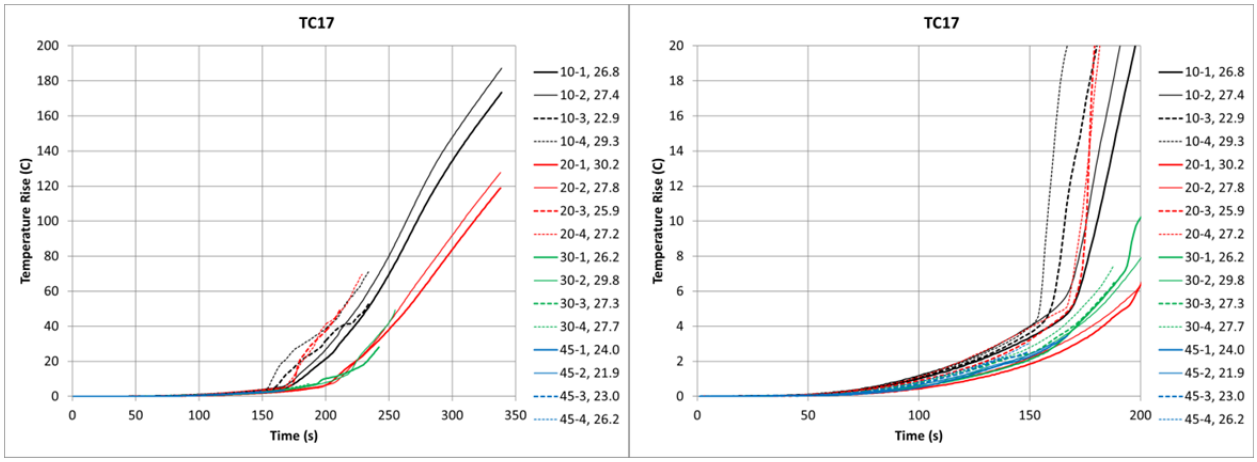

Figure 17: TC17 response for all tests, full temperature and time scale on left, zoomed in to examine initial temperature rise on right.

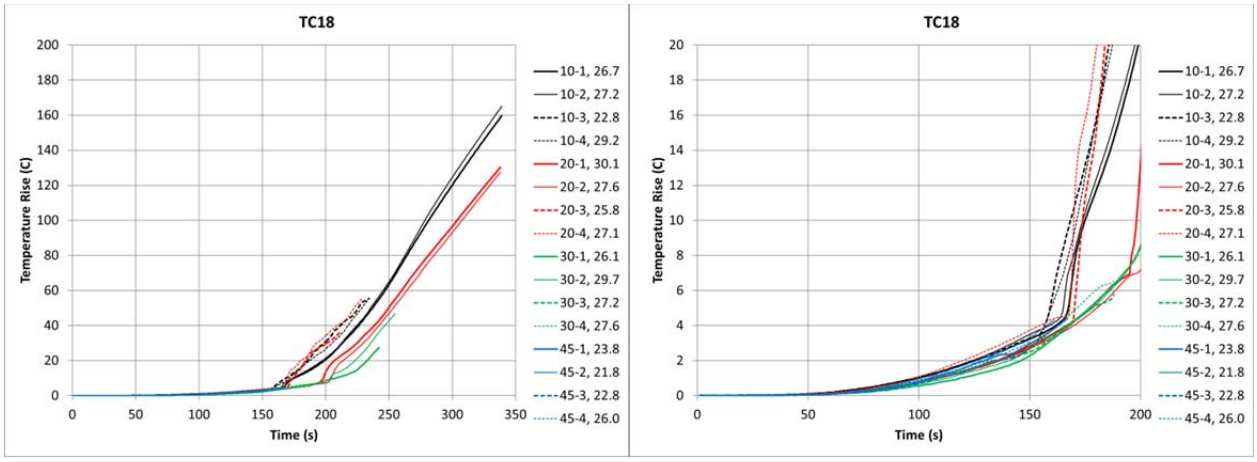

Figure 18: TC18 response for all tests, full temperature and time scale on left, zoomed in to examine initial temperature rise on right.

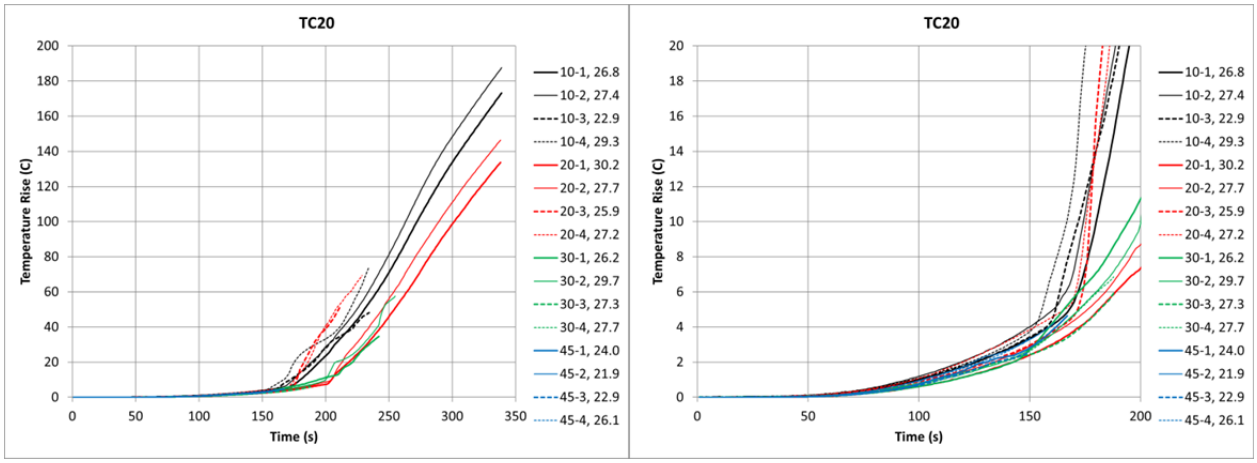

Figure 19: TC20 response for all tests, full temperature and time scale on left, zoomed in to examine initial temperature rise on right.

Figure 20 shows pressure measurement versus time. As discussed earlier (Figure 4), there is remarkable consistency between replicate tests (with exception of TDI20-3 and TDI20-4). While the thermocouples on the can edges exhibit excursions due to episodes of the hot product movement, the pressure is more of a bulk response for the whole apparatus and, correspondingly, small local events in the decomposition process are averaged out.

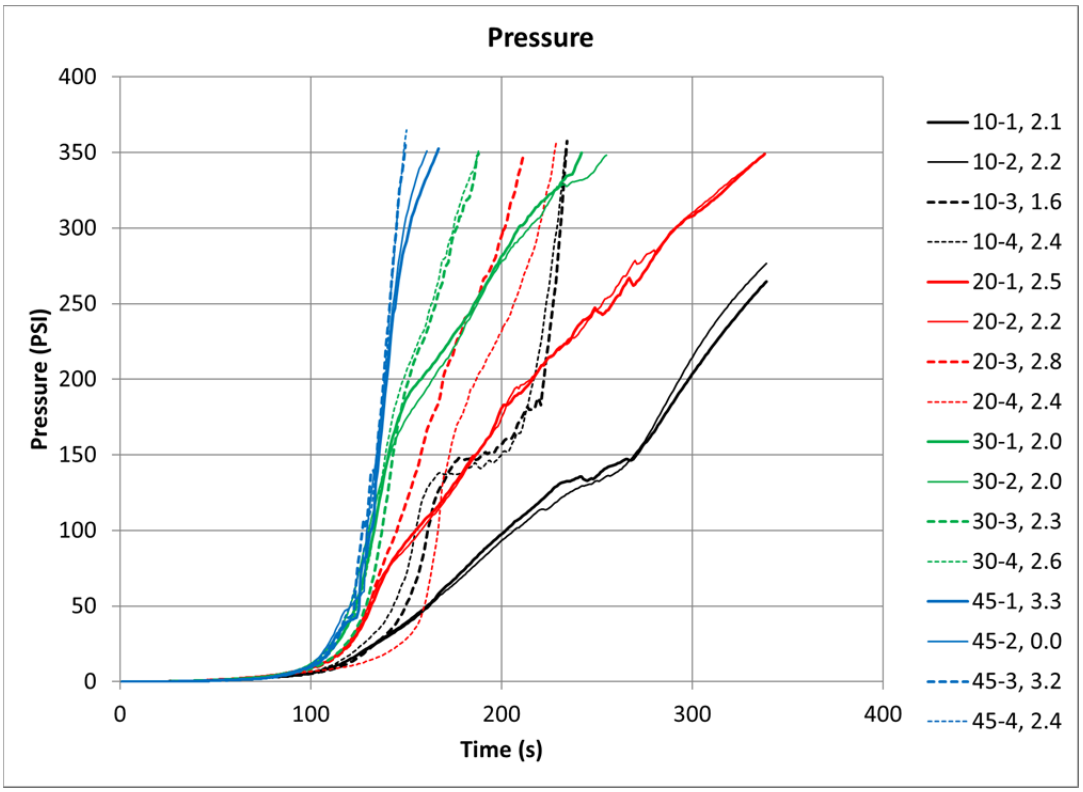

Figure 20: Measured pressure response for all tests.

4. THERMAL MODEL DESCRIPTION

Figure 21 and Figure 22 show the solid geometry and mesh for the thermal model, respectively. Also shown in the figure are Swagelok fittings for the plug and the pressure transducer line connection. The model substituted hollow circular cylinders of the same total volume and thermal mass but lacking the geometric details. The basic mesh shown in Figure 22 is comprised of approximately 35k tetrahedral elements. Results presented in this document used uniform mesh refinement resulting in approximately 216k elements (M1). A mesh resolution study is discussed in Section 5. Table 3 summarizes nominal material properties used in the model (adjustments to incorporate property uncertainty are discussed in a later section).

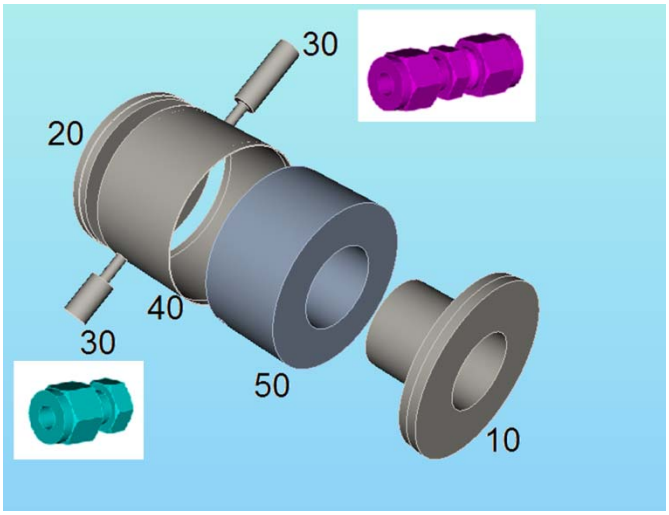

Figure 21: Blocks in the ARIA Model.

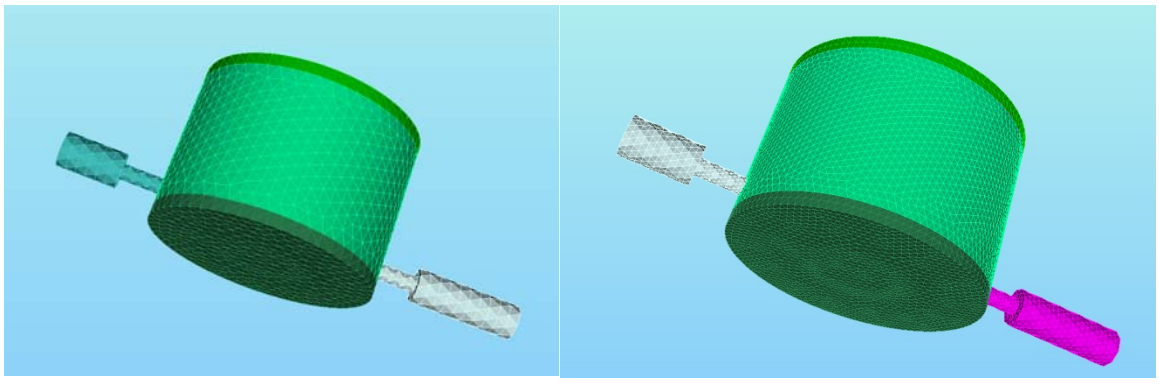

Figure 22: Base mesh (M0, 35k elements) and once refined (M1, 282k elements).

Table 3: Summary of material properties

Parts	Material	Description
Encapsulant (50)	TDI foam	Seven species, 2 step reaction model governs conversion from unreacted foam to char residue. Gaseous reactant species result in pressurizing constrained volume. Model development is described in Ref. [2]
Component, Top Plate, Bottom Plate (10, 20)	304 stainless	Constant density, temperature-dependent thermal conductivity and specific heat.
Sides, tubes, fittings (30, 40)	321 stainless	Constant density, temperature-dependent thermal conductivity and specific heat.

Boundary Conditions

The initial temperature for the model is uniform. Each of the sixteen unique foam densities and recorded lid control temperature histories (TC2) were used in the models. For each experiment, the initial temperature was taken to be the average of the initial thermocouple measurements at the start of the experiment.

Figure 23 shows four sidesets that were defined for the specification of boundary conditions. The bottom, sides, and tubes (sidesets 200, 300, and 400) were specified as convecting and radiating to a reference ambient temperature equal to the initial temperature of the system. The emissivity and convective coefficient are uniform over these surfaces with nominal values of 0.39 (Ref. [4]) and 10 $W/m^2 \cdot K$. Modeling the convective coefficient as constant and uniform is a compromise in order to keep the model tractable. Clearly, the natural convection that results around the transiently heated, 3-dimensional geometry is neither constant nor uniform. Using the can diameter as the length scale and the largest temperature difference occurring in the experiment to estimate the Rayleigh Number, correlations for spheres and up-facing horizontal surfaces all produce estimates of convective coefficient in the range of 9.5 to 10.5 $W/m^2 \cdot K$. A separate convective specification for the tubes (sideset 400) was considered but was not necessary as the tubes do not have a significant impact on simulation results due to the short duration of the experiments (this will be discussed later).

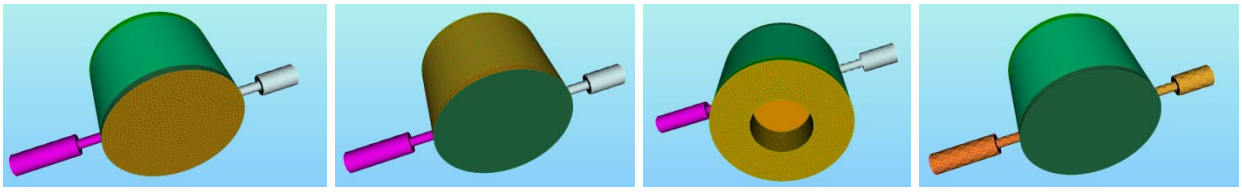

Figure 23: Sidesets 4, 200, 300, and 400 (copper highlighted in each view).

The remaining exterior surface, sideset 4, has a direct view of the heating lamps and thermal radiation is clearly the dominant mechanism for coupling of the heated surface to the energy source. The lamp pitch is small relative to the separation from the lamp plane from the can surface so that the center of the top "sees" several lamps. The lamp radiation source is idealized

as a uniform enveloping radiation surface of time-varying temperature. A user plugin was developed for use with ARIA [4] to implement a PID controller scheme to regulate this radiating temperature to produce the specified temperature history in the lid of the can. (Refer to Figure 3, the measured TC2 histories were used to produce a piece-wise linear temperature specification for each test.) The error condition is defined according to difference from a desired schedule:

$$e(t) = T_S(t) - T_C(t) \qquad (1)$$

where the terms on the right are the scheduled temperature and the control temperature, TC2 in the model. The schedule temperature, $T_S(t)$, is implemented in a piece-wise linear fashion from the series of time-temperature points included in the ARIA input. In the event that the analysis time exceeds the last time defined, the scheduled temperature is taken to be the last temperature specified in the input.

During the solution the reference radiation temperature, T_{ss4}, was set to:

$$T_{ss4}(t) = 850 + 30 \times e(t) + 0.5 \times \int_0^t e(t^*)\, dt^* \quad \text{(K \& s temperature \& time units)} \qquad (2)$$

The plug-in accommodates the constants appearing in the previous equation (as well as an additional constant multiplying $\frac{de(t)}{dt}$, which was not used (i.e., =0) in these analyses).

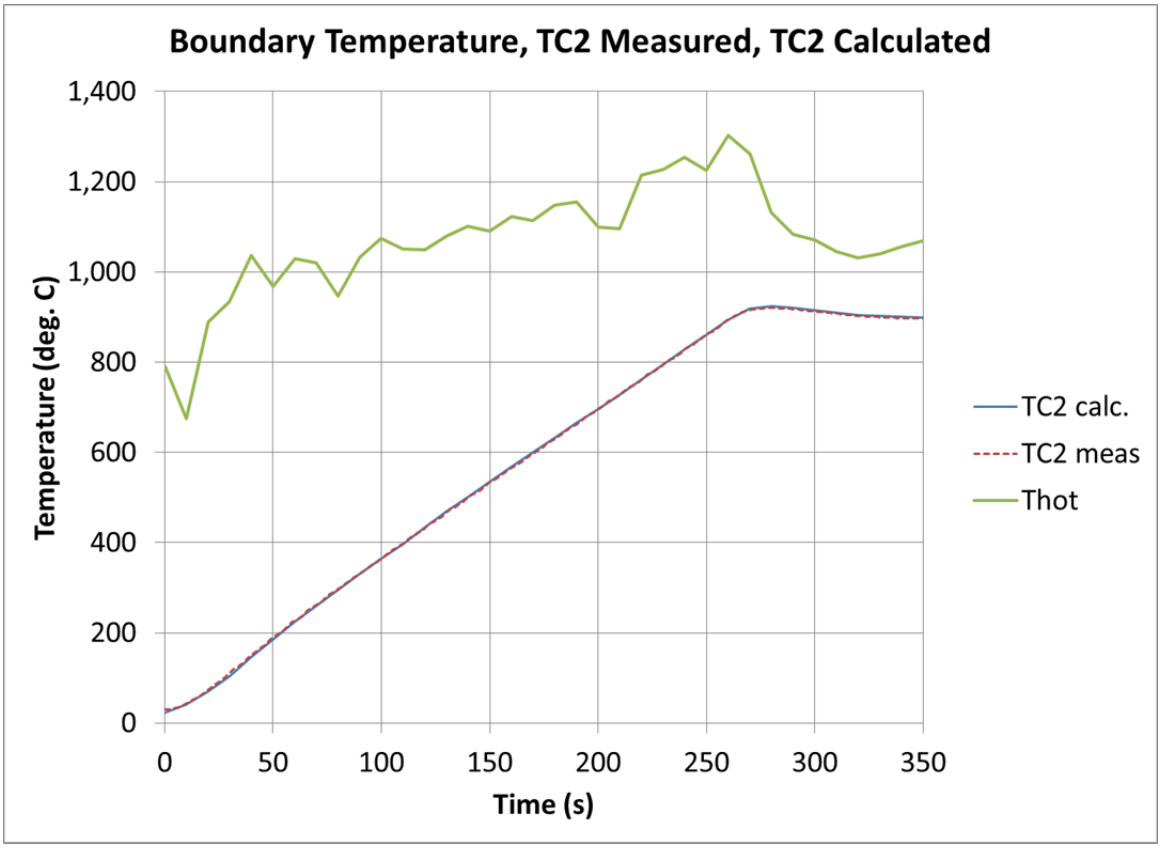

Figure 24: TC2 Measured, TC2 model result and controlled environment temperatures (T_{hot}) for TDI10-1 conditions.

Figure 24 shows the schedule temperature, the resulting response, and time-varying boundary temperature for this control scheme for the case of nominal model parameters and the TDI10-1 experiment. This control scheme provided an effective means to impose the measured temperatures at the boundary. Figure 25 shows the system temperature contours at 200s with the legend scale chosen to show the radial gradient in the lid (much of blue is "saturated" at temperatures below the bottom temperature indicated on the scale).

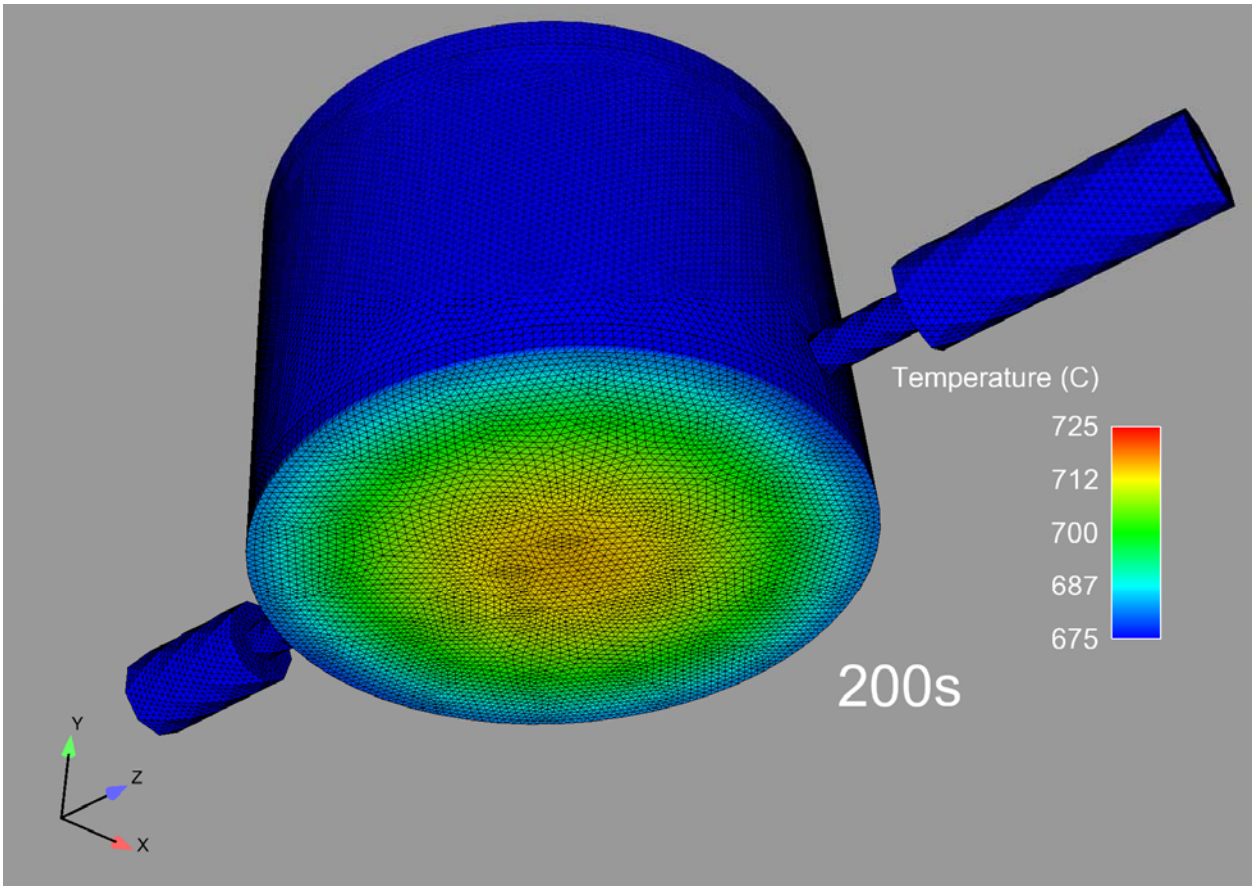

Figure 25: System temperature contours for TDI10-1 conditions at 200s, scale set to show radial gradients in lid (M2, 2.35M elements).

Recall (Figure 4) that the experiments last approximately 4 and 7 minutes (for inverted and upright geometry). The available measurements were compared to model predictions at the corresponding locations. Responses at those locations depend upon various parameters in the boundary conditions, properties affecting transient thermal conduction, and the foam response.

Developing understanding of the impact of the foam model in future applications is of immediate interest. The importance of foam component responses in general systems depends upon geometry, heating rates, and properties of the neighboring components in the system. As transient heat conduction predictions are relatively mature, the present experiments were designed to produce responses that are strongly dependent on the foam's behavior. Ideally, the foam model will demonstrate the onset and rate of decomposition and transport through

converted foam consistent with experimental observation. These experiments generally ran long enough to produce a response in the component (TC18).

From Figure 4, it is apparent the orientation of the can has an important effect on the pressure response. Discussions in References [1-3] postulate that the more rapid building of pressure in the can for the inverted geometry is due to the liquid phase produced during decomposition moving towards the heated surface and reacting immediately to produce gases, as compared to the upright configuration where the liquefied decomposition products remain in the liquid phase. In addition, in the inverted orientation, convective heat transfer due to the moving liquid is significantly more pronounced than in the upright orientation. From these features, it is evident that gravity has an important influence on the system. From Figure 4, it is shown that the separation in pressure responses between upright and inverted orientations occurs at higher pressures for higher density foams.

The current model has known deficiencies because it does not include the aforementioned dependence on orientation in gravity. Uncertainty Quantification analysis is performed on the existing model to learn which of its parameters is most significant in determining the results. It is of particular interest to compare the quantified uncertainty of the model to the differences in measured responses attributed to orientation. If the model uncertainty is large relative to the differences in response attributed to orientation, the implication is that the dividends for pursuing more complete model are reduced.

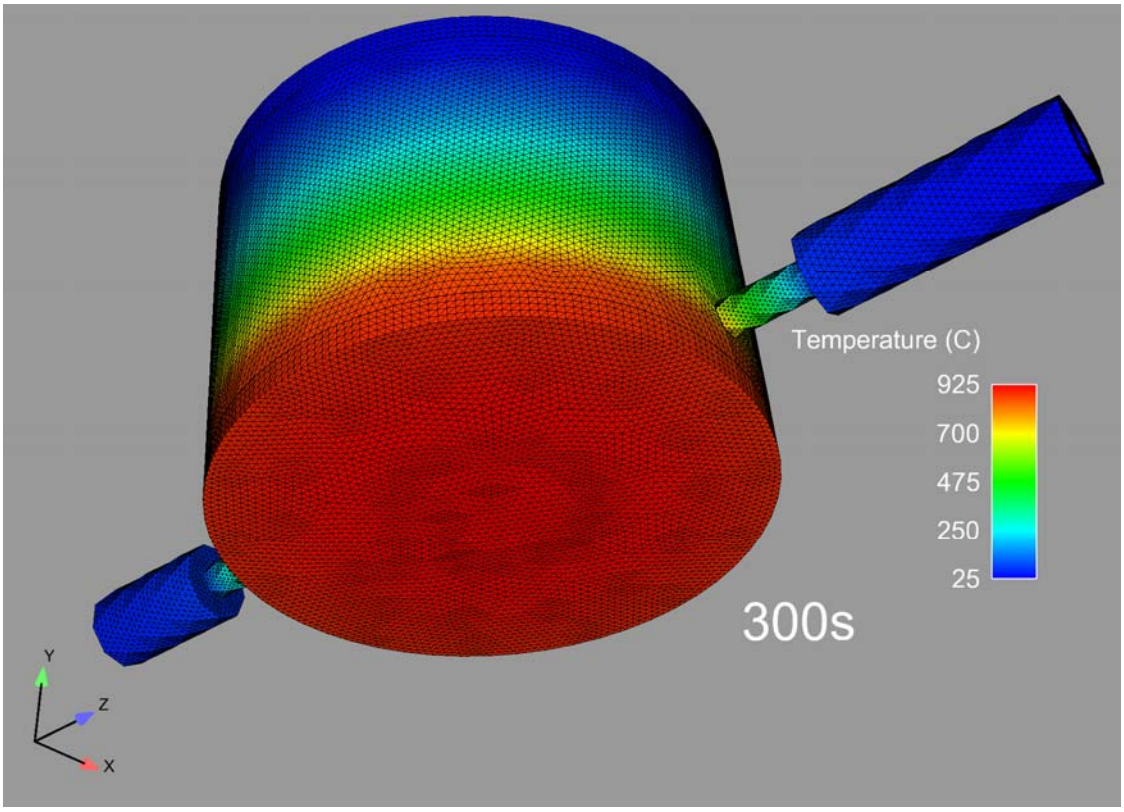

Figure 26: Predicted temperature distribution at 300s, 10lb/ft^3 foam, Upright 1 conditions (M2, 2.35M elements).

Figure 26 shows the predicted temperature contours for the conditions of TDI10-1 at 300s (note that most of the tests were shorter than 300s). Note that the fittings have not experienced any appreciable increase in temperature. Conditions for discharge line continuing from the connecting fitting were not characterized or controlled precisely enough to implement detail of its influence on the system. Figure 26 demonstrates that the boundary condition details past the fittings are of little consequence.

5. MESH STUDY

The uniform mesh refinement feature available in ARIA was applied to study the effect of mesh size on predicted responses for 600s (well past the time of any of the tests) of heating for the "Upright 1" test case for each of the foam densities. Meshes used were those shown in Figure 22 (35k elements, M0), that mesh uniformly refined (282k elements, M1), and that mesh uniformly refined twice (2.35M elements, M2). M2 is shown in Figure 25 and Figure 26. The base mesh shown in Figure 22 was developed using Cubit with the tetmesh scheme and an "approximate size" for all blocks of 3 mm. Other than the regulated temperatures (TC1-TC4) in the lid, all of the variables in the analysis increase monotonically until the end time of the analysis.

Table 4 summarizes mesh dependence of variable value at 600s for the TDI10-1 test boundary conditions for each of the nominal foam densities. For these cases, the analysis was completed for each of the M0, M1, and M2 meshes. Richardson extrapolation ($f = 4/3 f_{\text{fine}} - f_{\text{coarse}}/3$) estimates using the M0 and M1 mesh (R0_1) and the M1 and M2 mesh (R1_2) were also calculated based on assumed second order convergence rate and the uniform halving of the elements in each direction [7]. The percent deviation for each mesh for each variable in Table 4 is calculated based on R1_2, theoretically the most accurate of the estimates.

Figure 27 shows the transient response prediction using the various meshes for TC18. The coarsest mesh (M0) result stands alone. In Table 4 M0 results are 4-7% off from the reference for the four densities at the end time of the analysis. The R0_1 legend entry designates Richardson extrapolation using M0 and M1. The R1_2 legend entry designates Richardson extrapolation using M1 and M2. M1, M2, and the Richardson extrapolations are barely distinguishable.

Figure 28 shows the results for the meshes and extrapolations for the pressure prediction. Figure 27 and Figure 28 are typical results. Similar plots were inspected for all the foam densities and various locations and it is consistently the case that the results from the coarse mesh varied from the rest which were nearly coincident. These results demonstrate that the M1 mesh is sufficient for the current study.

Table 4: Comparison of terminal variable value for three meshes. All four nominal densities were used with the TDI10-1 test boundary conditions.

Variable	10 lb/ft^3 foam			20lb/ft^3 foam			30 lb/ft^3 foam			45 lb/ft^3 foam		
	δ% M0	δ% M1	δ% M2	δ% M0	δ% M1	δ% M2	δ% M0	δ% M1	δ% M2	δ% M0	δ% M1	δ% M2
TC1	0.2	0.2	0.0	0.1	0.0	0.0	0.1	0.1	0.0	0.1	0.0	0.0
TC2	0.1	0.1	0.0	0.0	0.0	0.0	0.1	0.1	0.0	0.0	0.0	0.0
TC3	0.1	0.1	0.0	0.0	0.0	0.0	0.1	0.1	0.0	0.0	0.0	0.0
TC4	0.1	0.1	0.0	0.0	0.0	0.0	0.1	0.1	0.0	0.0	0.0	0.0
TC5	1.9	0.8	0.2	2.0	0.8	0.2	2.6	1.1	0.3	5.4	2.2	0.5
TC6	0.9	0.4	0.1	1.3	0.6	0.1	2.3	1.0	0.3	4.5	1.8	0.4
TC7	1.8	0.6	0.2	2.6	1.0	0.2	3.5	1.3	0.3	4.1	1.5	0.4
TC9	1.5	0.6	0.1	1.6	0.6	0.2	2.0	0.8	0.2	4.3	1.8	0.4
TC10	0.6	0.3	0.1	1.1	0.5	0.1	2.2	0.9	0.2	4.1	1.6	0.4
TC11	0.7	0.1	0.0	1.3	0.4	0.1	2.0	0.7	0.2	2.3	0.8	0.2
TC13	9.1	3.8	0.9	10.3	4.3	1.1	11.6	4.9	1.2	10.3	4.1	1.0
TC14	8.8	3.6	0.9	10.0	4.1	1.0	11.3	4.8	1.2	10.2	4.0	1.0
TC15	8.8	3.6	0.9	9.9	4.1	1.0	11.2	4.7	1.2	10.0	4.0	1.0
TC16	8.9	3.6	0.9	10.0	4.1	1.0	11.4	4.8	1.2	10.3	4.1	1.0
TC17	4.8	1.7	0.4	5.0	1.8	0.4	6.4	2.7	0.7	7.3	2.8	0.7
TC18	4.4	1.6	0.4	4.6	1.7	0.4	6.0	2.7	0.7	6.8	2.8	0.7
TC20	5.1	1.8	0.5	5.4	2.0	0.5	6.8	2.9	0.7	7.7	3.2	0.8
Pressure	-1.7	-0.6	-0.2	-2.0	-0.8	-0.2	-3.2	-1.3	-0.3	-5.3	-1.8	-0.5

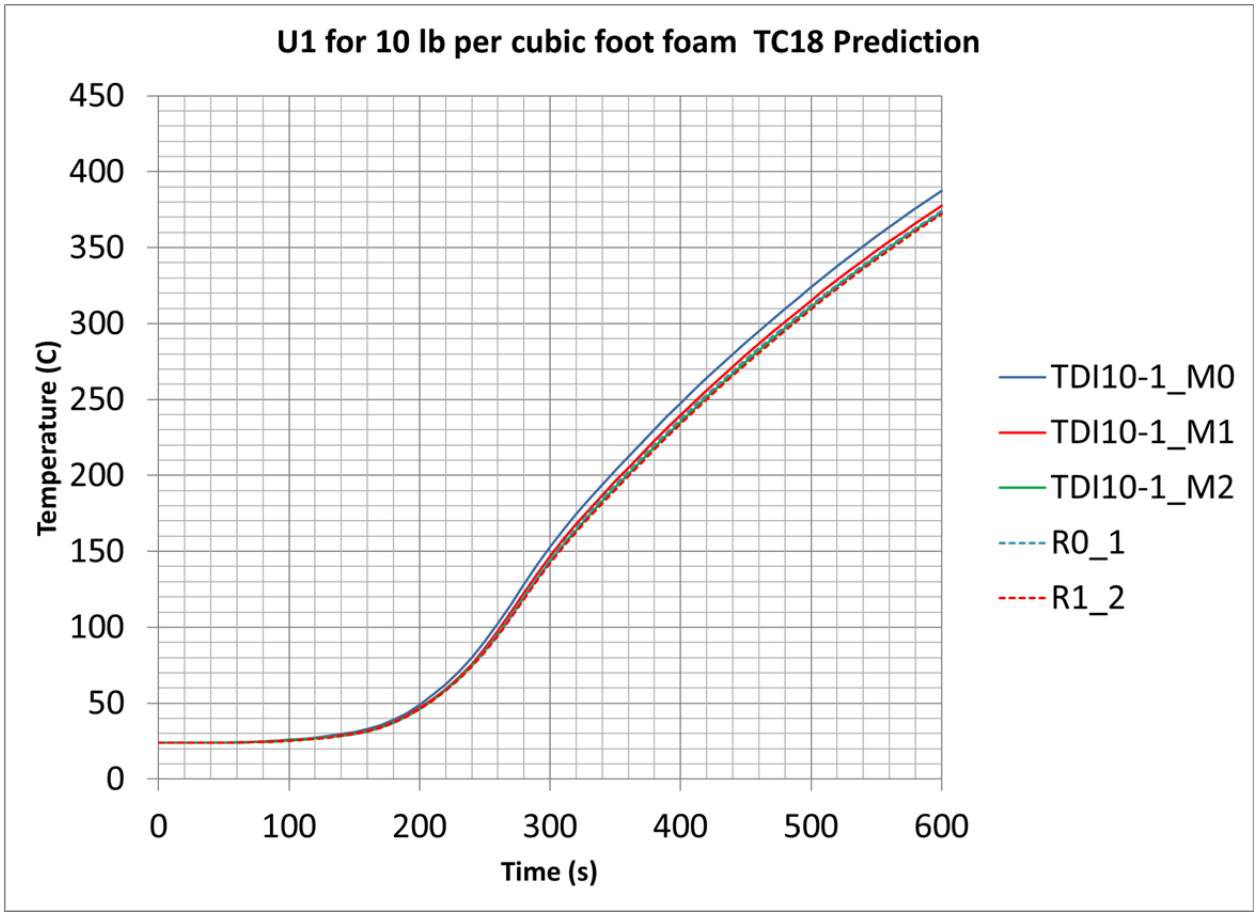

Figure 27: Transient response for TC18 comparing results for basic mesh and two levels of refinement with Richardson interpolation (dashed lines).

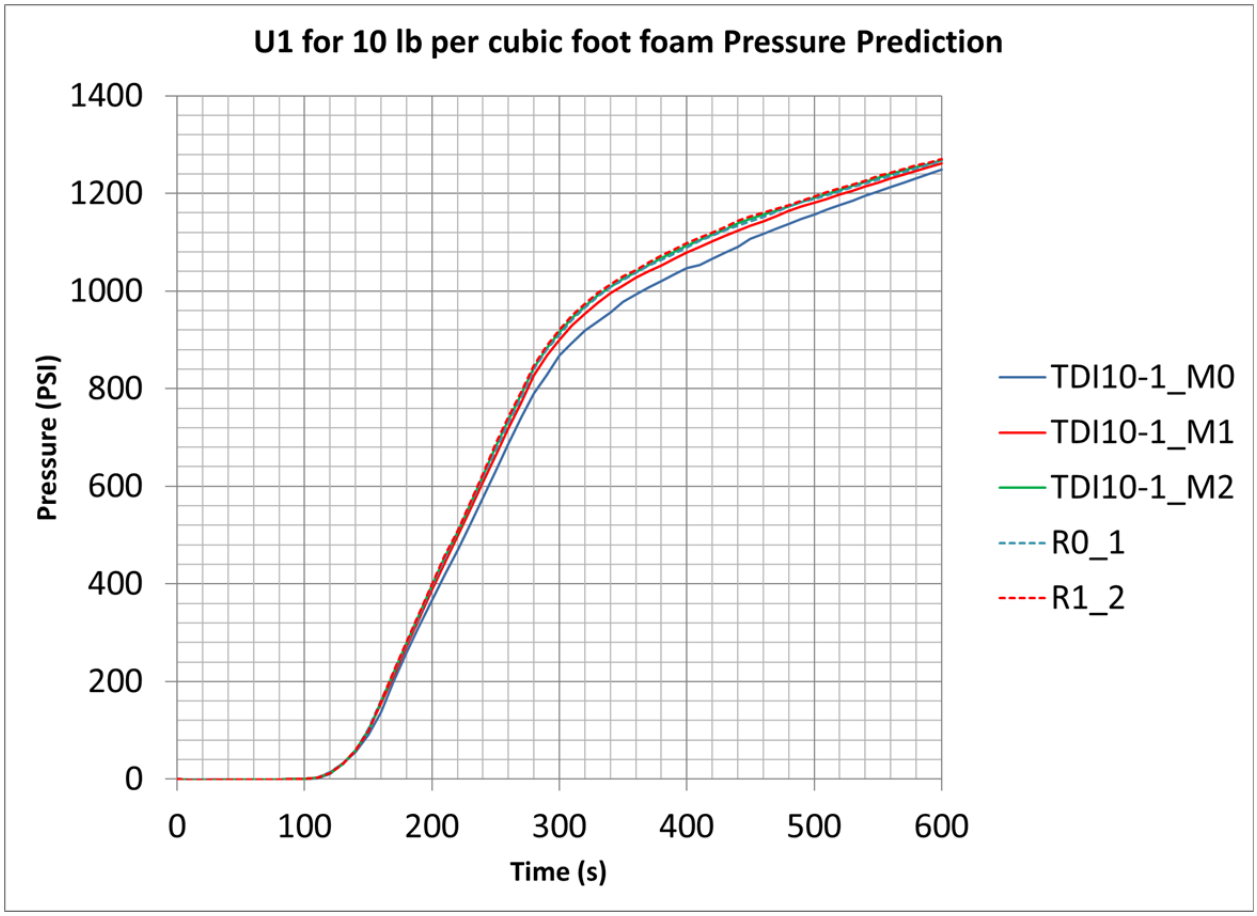

Figure 28: Transient pressure prediction comparing results for basic mesh and two levels of refinement with Richardson interpolation (dashed lines).

6. UNCERTAINTY QUANTIFICATION METHOD

The mean value method was used to propagate uncertainty through the model. In the next section, specific parameters are identified and the results of applying the mean value method are described and assessed. In order to introduce a consistent nomenclature, a brief, general description of the method is included here. Let a vector representing mean values of N parameters of interest to the problem be:

$$\bar{p} = \{p_1, p_2, p_3 \ldots p_N\}. \quad (3)$$

The members of $\bar{p}$ are quantities that occur in the model such as thermal properties. It is convenient to normalize the physical parameters by their expected mean values and define dimensionless parameters as:

$$\bar{P} = \{P_1, P_2, P_3 \ldots P_N\} \quad (4)$$

so that each parameter (P_i) is dimensionless and of unit value when it is at its expected value.

A vector of M responses is:

$$\bar{R} = \{R_1, R_2, R_3 \ldots R_M\}. \quad (5)$$

The responses are predicted quantities of interest. For the current effort, responses are measured temperatures and pressure. All of the dimensionless parameters ($\bar{P}$) are constant through a model run and the responses are functions of time. When properties are temperature-dependent, i.e., thermal conductivity, $k(T) = P_k k_{\text{nom}}(T)$.

The *sensitivity* of the j-th response to the i-th parameter is estimated by central differencing as:

$$\frac{\partial R_j}{\partial P_i} \approx \frac{R_j(\bar{P}+\delta P_i) - R_j(\bar{P}-\delta P_i)}{2\delta P_i} \quad (6)$$

Where $R_j(\bar{P} + \delta P_i)$ and $R_j(\bar{P} - \delta P_i)$ represent the j-th responses for the system with the i-th parameter incremented up by δP_i and down by δP_i respectively. As P_i is dimensionless, the sensitivity has the same units as the corresponding response variable. For example, if the response is a temperature (°C), its sensitivity with respect to a (dimensionless) parameter is the change in temperature (°C) per fractional change in the parameter.

Estimates of the standard deviations of the parameters are represented by the vector:

$$\bar{\sigma} = \{\sigma_1, \sigma_2, \sigma_3 \ldots \sigma_N\}. \quad (7)$$

The variance for the system response considering all the parameter uncertainties is estimated as:

$$\sigma_{R_j}^2 = \sum_{i=1}^{N} \left(\frac{\partial R_j}{\partial P_i}\sigma_i\right)^2 \quad (8)$$

Dividing by $\sigma_{R_j}^2$ gives a relative contribution of each parameter to the normalized variance:

$$1 = \left(\frac{\partial R_j}{\partial P_1}\frac{\sigma_1}{\sigma_{R_j}}\right)^2 + \left(\frac{\partial R_j}{\partial P_2}\frac{\sigma_2}{\sigma_{R_j}}\right)^2 + \cdots + \left(\frac{\partial R_j}{\partial P_N}\frac{\sigma_N}{\sigma_{R_j}}\right)^2 \quad (9)$$

and

$$I_{ij} = \left(\frac{\partial R_j}{\partial P_i}\frac{\sigma_i}{\sigma_{R_j}}\right)^2 \quad (10)$$

is the *importance* of the i-th parameter to the j-th response. The importance factor is defined by normalizing Eq. 8 by the total variance, as a result, the sum of the importance factors for all parameters equals one. Each importance factor represents the fraction that a parameter contributes to the total variance. Figure 29 and Figure 30 include plots of the sensitivities and importance of parameters for the response predicted at the TC5 location for the conditions of TDI20-1. Note that each sensitivity and importance factor is evaluated at each point in time for the transient analysis.[2] Very early in time, before any real system response, importance for TC5 is only associated with the environmental temperature because there has been no time for energy to diffuse to TC5, but the environment is tied to the location from time zero through the

[2] The rationale for choosing parameters for study and their magnitudes will be addressed in a following section. The immediate purpose is to discuss the character of results predicted by the method.

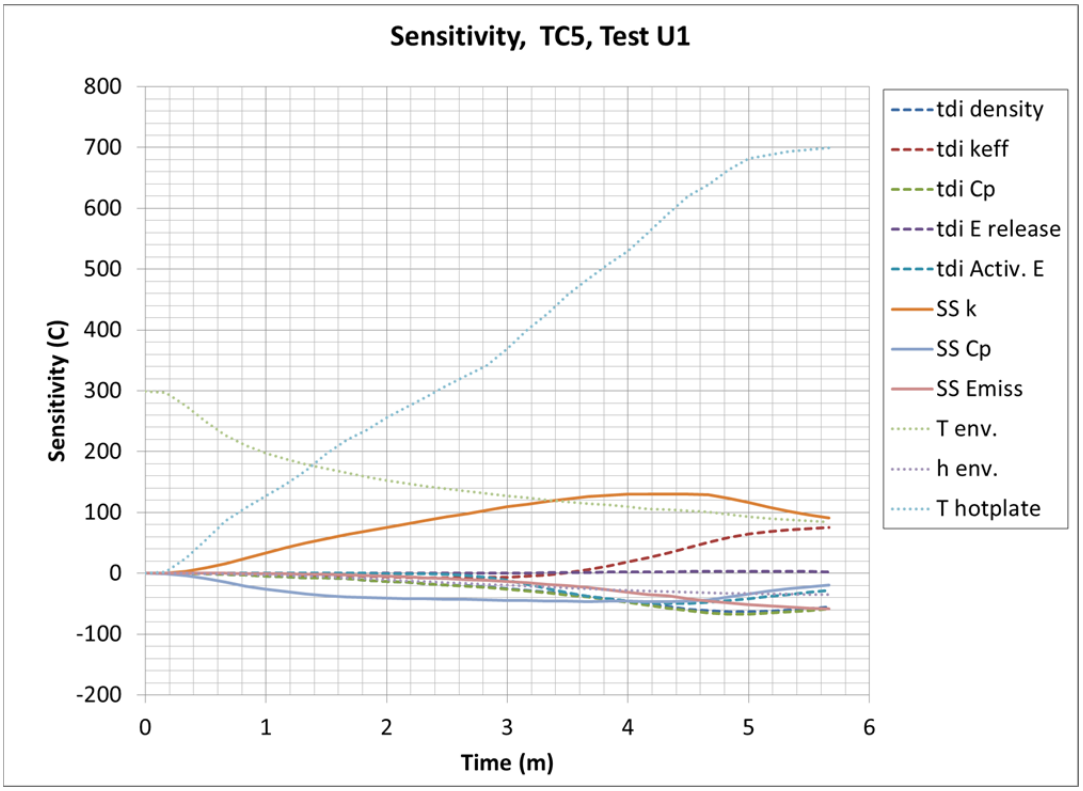

Figure 29: Sensitivity of TC5 to various parameters, TDI20-1 conditions.

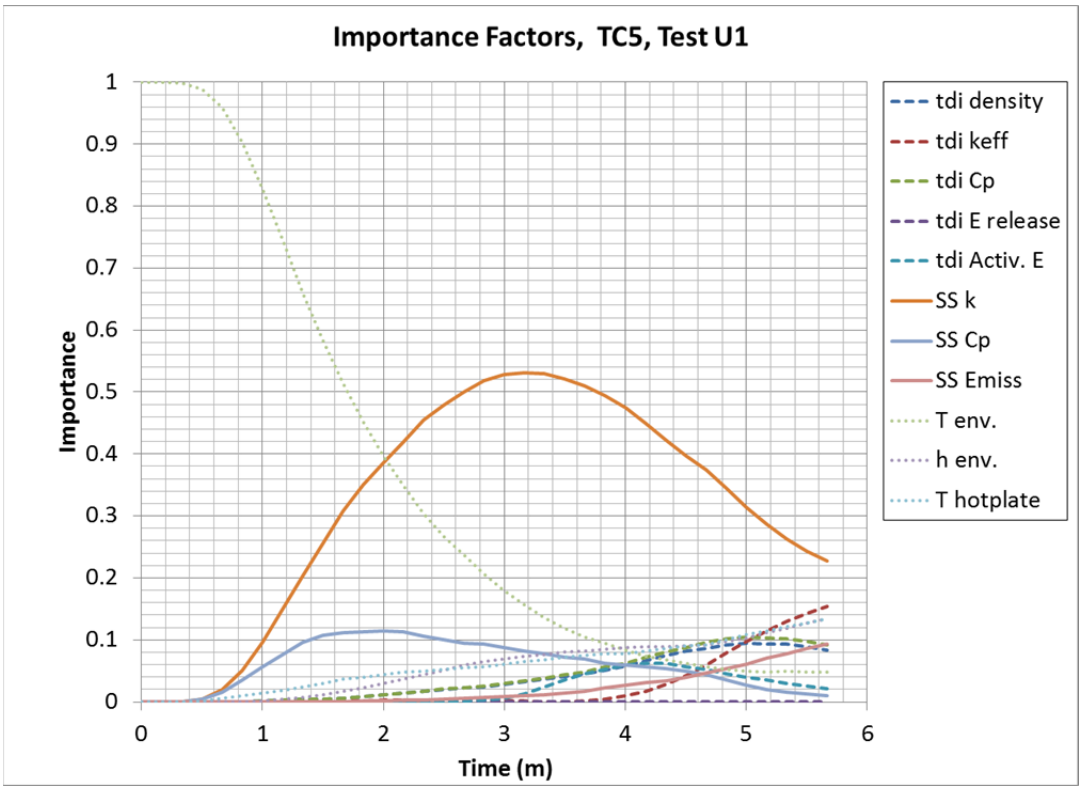

Figure 30: Importance of various parameters to of TC5, TDI20-1 conditions.

convective boundary condition. At approximately 3 minutes (Figure 30) the thermal conductivity of the can becomes most important to the response. By the end of the analysis, the importance of the thermal conductivity decreases and the effective conductivity of the foam becomes important as the location is increasingly influenced from the interior side of the can.

Figure 31shows the measured response at TC5 (green bars) and the model-predicted response shown as the solid blue line and blue error bars bounding the 95% confidence interval where the variance in the prediction was estimated according to Eq. 8. Figure 32 shows the model result minus the measurement with the error bars indicating total error including measurement error as defined in Eq. 11.

$$\sigma_{tot}^2 = \sigma_{TC5}^2 + \sigma_{meas}^2 \qquad (11)$$

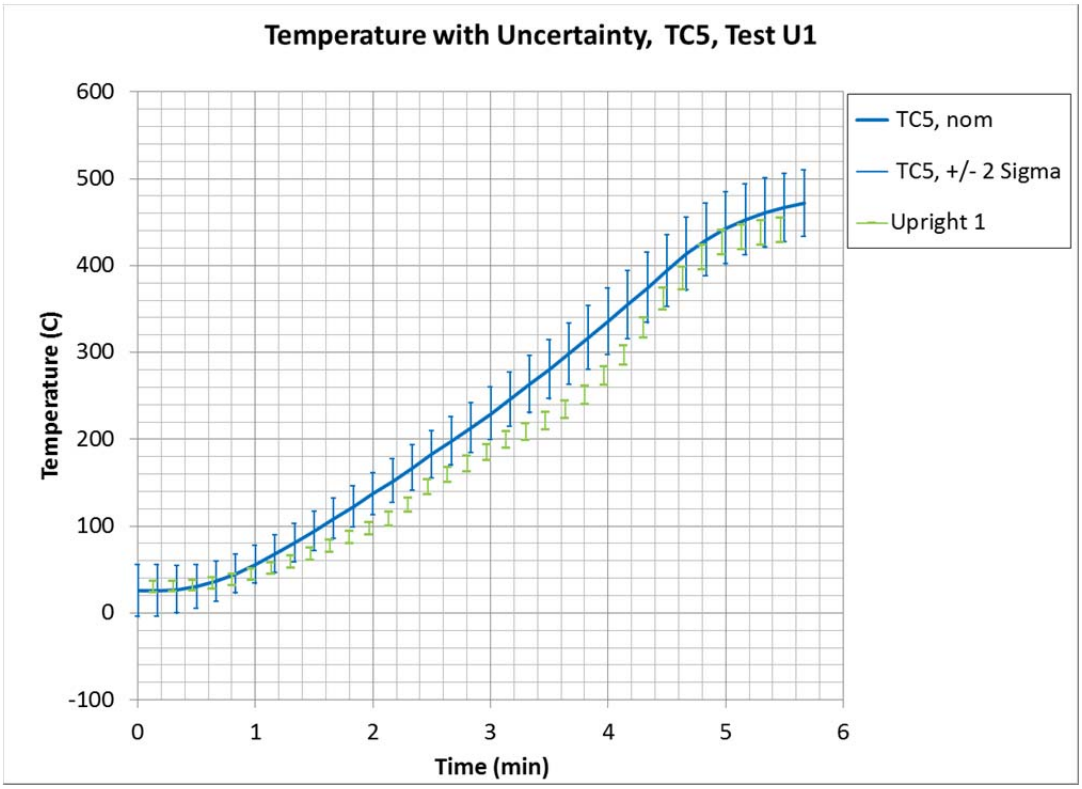

Figure 31: TC5 predicted temperature response with 95% confidence intervals and measured response for conditions of TDI20-1.

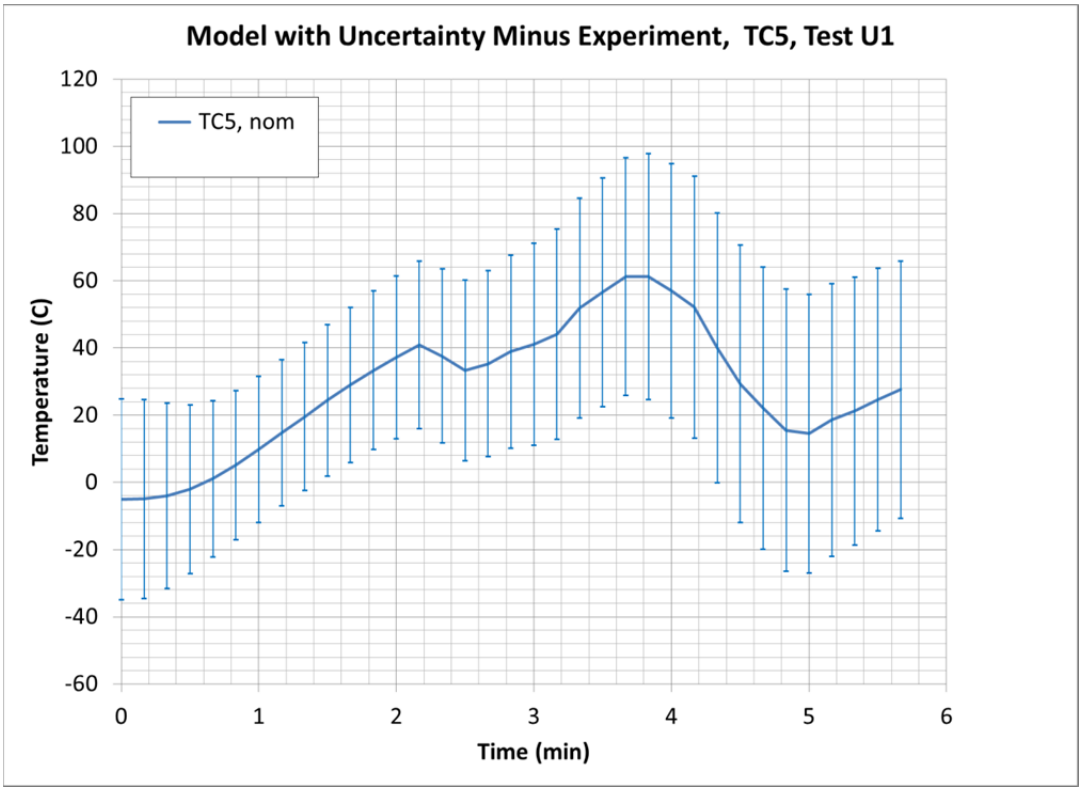

Figure 32: TC5 predicted temperature response in excess of measurements with 95% confidence intervals for conditions of TDI20-1.

Figure 29 through Figure 32 demonstrate various views of the UQ analysis. In the case presented (TC5 TDI20-1) the model prediction is narrowly unsatisfactory insofar as the predicted confidence intervals to do not fully enclose the measurements (Figure 31). In the view presented in Figure 32, the nominal expectation of the model is that the uncertainty interval at all points of time surround zero.

Additional views of the modeling results, such as estimation of the time to specified responses, have also been considered. With numerous tests, several parameters, and several response locations of interest the number of such plots becomes unwieldy and more compact measures are desired. Additional metrics were formed using the importance parameters to filter out parameters that exhibit importance during times where no response has occurred. The simple time average of an importance factor for the experiment is:

$$\bar{I}_{ij} = \frac{1}{T}\int_0^T I_{ij}dt, \qquad (12)$$

where T is end time for the analysis, is the average value of the importance I_{ij}. $\bar{I}_{ij}$ can be calculated from the information in Figure 30 to suggest an overall ranking ordering of the importance of parameters for the problem. $\bar{I}_{ij}$ may include a significant time interval for which no response has occurred and, consequently, be misleading. An additional quantity was calculated as follows:

$$\check{I}_{ij} = \frac{1}{TR_{j,max}}\int_0^T \left|R_j(t) - R_j(0)\right| I_{ij}\, dt \qquad (13)$$

$\check{I}_{ij}$ is a time-averaged-response-weighted version of importance which accrues value during the transient only when response is coincident with importance. For the information in Figure 30, this definition of importance will appropriately disregard the importance associated with the environment temperature in that it occurs before TC5 actually responds.

7. PARAMETERS CONSIDERED IN UQ ASSESSMENT

Table 5 summarizes the parameters that were considered in the mean value method assessment of UQ. Properties associated with the foam are described in Ref. [2]. As noted earlier, parameters of the UQ method are constant through an analysis. The effective conductivity in the thermal model is a strong function of temperature, but the corresponding UQ parameter is the unit multiplier in the case of the nominal value of the parameter or perturbed either direction by the δP_i (10%) indicated in Table 5 and the multiplier, $(1 \pm \delta P_i)$, modifies the function of temperature in the model. Similarly, $f_1(T)$ and $f_2(T)$ are tabular functions for the thermal conductivity and specific heat of stainless steel which are either unmodified (nominal) or multiplied by $(1 \pm \delta P_i)$.

Table 5: Summary of Parameters Varied in UQ Analysis.

Parameter name in graphs	Description/mean value	Std Dev of P_i (σ_i)	δP_i	Basis for σ_i
tdi density	Unreacted foam density, see Table 1.	0.1	0.1	Ref. [2]
tdi keff	Combined conductivity, conduction and radiation diffusion contributions.	0.1	0.1	
tdi Cp	$f_3(T)$ tabular function	0.1	0.1	
tdi E release	0.25MJ/kg (1st reaction only)	0.1	0.1	
tdi Activ E	207.85MJ/kg	0.1	0.1	
SS k	$f_1(T)$ tabular function	0.1	0.1	
SS Cp	$f_2(T)$ tabular function	0.1	0.1	
SS Emiss	0.39	0.1	0.1	Ref. [5]
T_{env}	Equal to system initial temperature	0.05	0.05	
h_{env}	10 W/m^2·K	0.2	0.2	Correlations
$T_{hotplate}$	Measured temperatures nominally 200°C/min. until @ 900°C	0.01	0.01	Measured

Since the measured lid temperature from the corresponding experiment was applied as a boundary condition in each experiment model, the associated uncertainty (0.01, Table 5) is the estimated measurement error.

8. UNCERTAINTY QUANTIFICATION ASSESSMENT RESULTS

For each of the tests, the numerical operations described in the preceding section were performed for the 11 parameters of Table 5 for nine response locations summarized in Table 6. The pressure rise in the can and the thermal response of the component (TC18) are of particular interest and additional representative transient plots will be presented for these two locations to

gain further insight into system/model behavior. The importance parameters as demonstrated in Figure 30 and as weighted integral quantities (defined in Equation 13) provide a valuable means of comparison.

Table 6: Summary of response locations considered.

Location	Comments
TC2	Control point in lid. Lid responses are generally disinteresting because the heater controller prescribed the response closely (see Figure 24).
TC5	Symmetric to TC9. Largely influenced by can conduction. Eventually heats from interior when foam has decomposed.
TC6	Symmetric to TC10. Largely influenced by can conduction.
TC7	Symmetric to TC11. Largely influenced by can conduction.
TC14	Nearly (due to vent tubes) symmetric to TC13, TC15, TC16. Largely influenced by can conduction. At this distant end of the can the convective connection to the environment is more significant.
TC17	Component response, largely tracks TC18 in both experiments and modeling.
TC18	Preferred (centered) component response location.
TC20	Component response, largely tracks TC18 in both experiments and modeling. Symmetric to TC17 and some asymmetry can be witnessed by comparison to TC17 in experimental results.
Pressure	Being a sort of bulk property of the reacting volume, pressure is generally less affected by local disturbances. Note the replicate test agreement in Figure 4.

Figure 33 and Figure 34 show the importance parameters for the pressure response for the upright configuration for 10 lb/ft^3 and 45 lb/ft^3 foams respectively. In both cases, the TDI activation energy is the important parameter as soon as pressure begins to build. Later in time, the TDI density also becomes an important parameter for the less dense foam but this effect is small in the 45 lb/ft^3 foam case.

Figure 35 and Figure 36 show the model prediction for pressure in the upright configuration along with the uncertainty intervals associated with the parameters of Table 5 for 10lb/ft^3 and 45 lb/ft^3 foam and for the denser foam, these uncertainty intervals capture the measurements. Note that for the denser foam the predictions are generally less than the measurement whereas those of the lighter foam are greater.

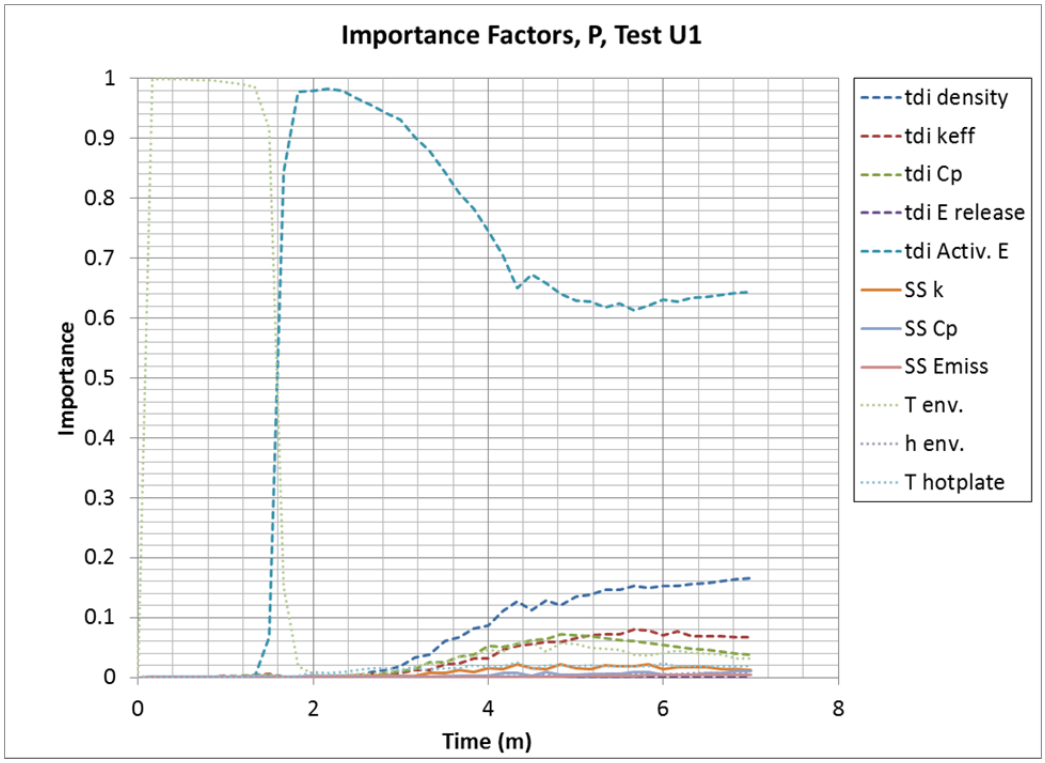

Figure 33: Importance factors for pressure for TDI10-1.

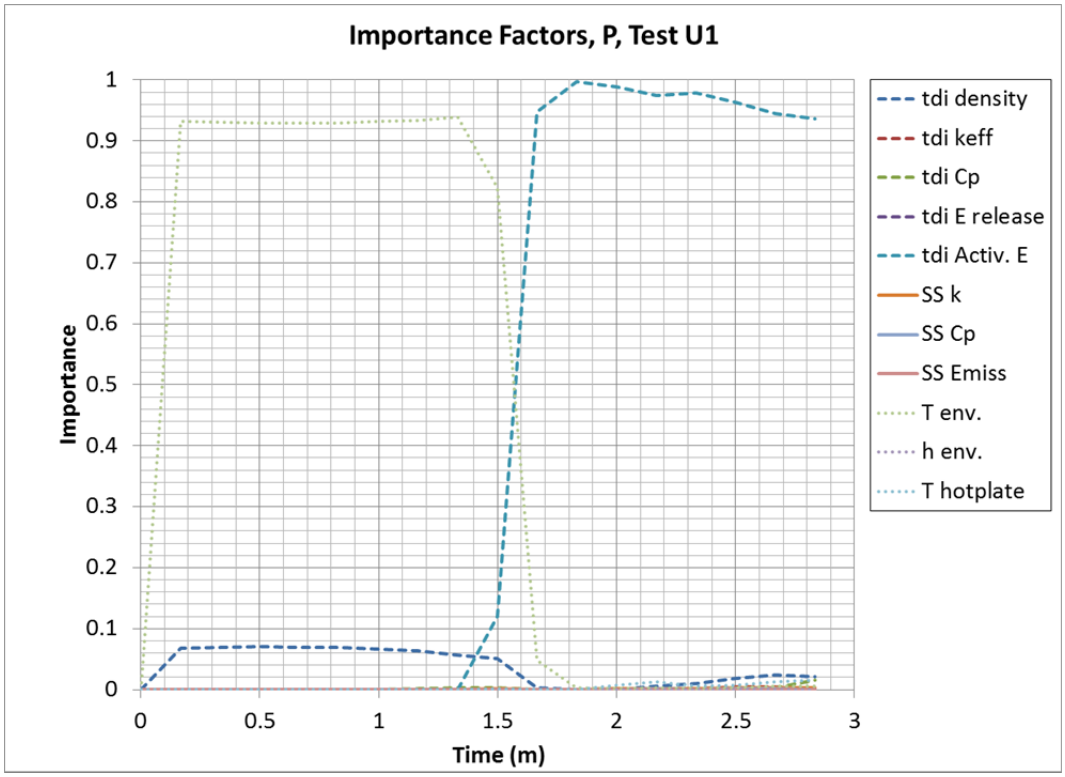

Figure 34: Importance factors for pressure for TDI45-1.

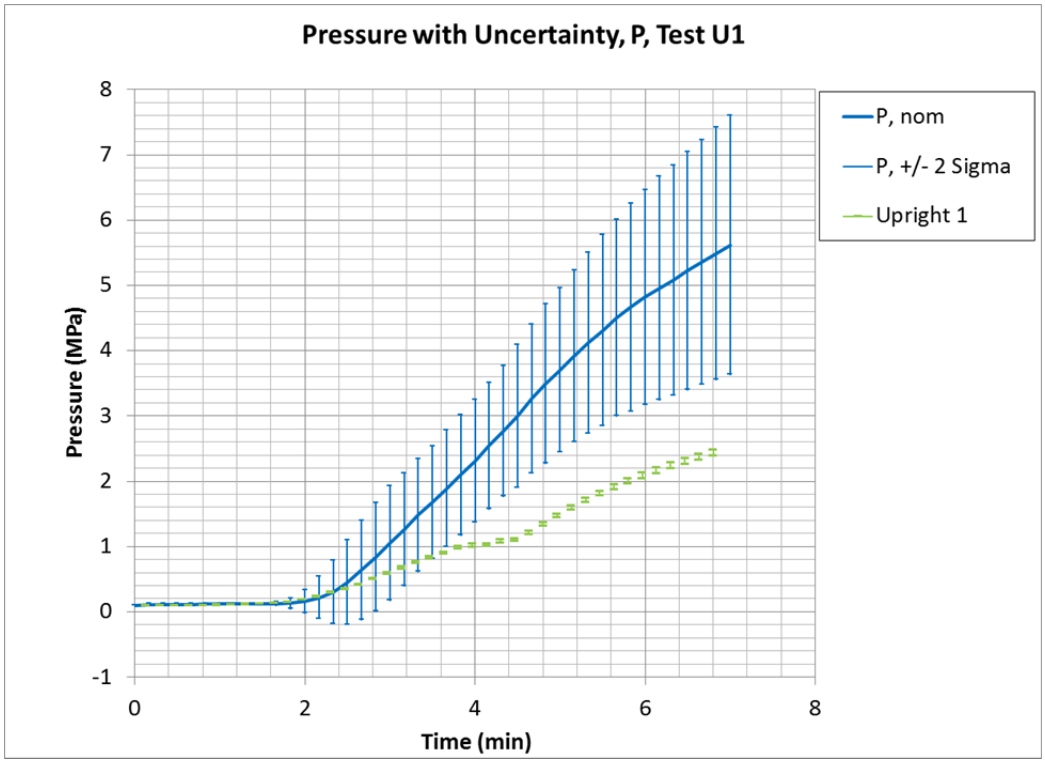

Figure 35: Model results with thermal parameter uncertainty and measured pressure for TDI10-1.

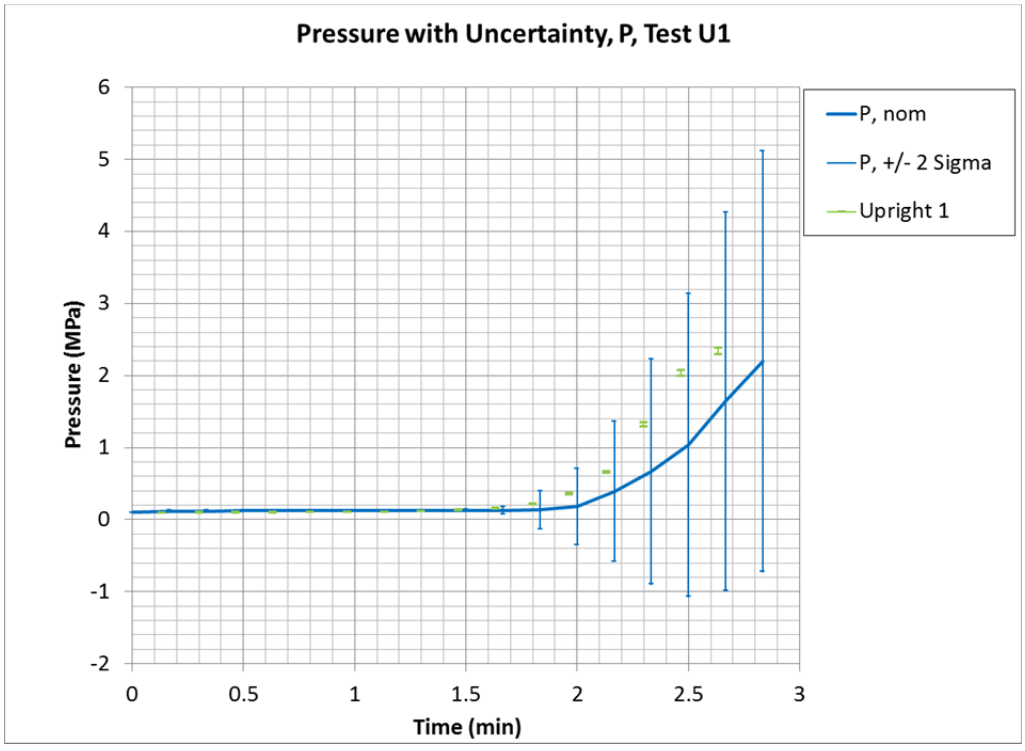

Figure 36: Model results with thermal parameter uncertainty and measured pressure for TDI45-1.

In the chemistry model, pressure increase is a result of gas product production due to pyrolysis reactions that occur because of an increase in temperature within a constrained volume. In the current model formulation, the transport properties in the model are independent of pressure, i.e., the simulation response is independent of the pressure response. Consequently, it was convenient to consider additional uncertainty for the pressure response outside of the model manipulated for UQ. The foam decomposition model has model form errors associated with it due to physics that are not incorporated into the model. To compensate, additional model form errors have been added to uncertainty in the pressure prediction. The model form errors aim to account for discrepancies in the volume that the gas occupies, the amount of material in the gas phase, the reaction temperature, and the temperature of the gas. The volume available to the gas is uncertain because the foam is initially closed cell and the pore structure opens as pressure and temperature increase. In addition, the formation of liquid and potentially a liquid layer influences the volume available to the gas. When TDI decomposes, it produces smaller polymer fragments that can be distributed between the gaseous and liquid phases depending upon pressure and temperature and a vapor-liquid equilibrium balance. In this model, thermal equilibrium between phases is assumed, and the heat transfer through the foam has errors associated with it, therefore the temperature at which reactions occur is uncertain, thus causing the moles of gas calculated to be uncertain. The magnitude of additional uncertainty was calculated as a multiplier based on the individual uncertainty contributions. Model form errors were assigned with minimum and maximum multipliers: the amount of material in the gas phase has a multiplier of 0.83 to 1, the temperature of the gas associated with the number of moles of gas produced has a multiplier of 0.8 to 1.2, the volume that the gas occupies has a multiplier of 0.83 to 1.0, and the temperature of the entire gas phase has a multiplier of 0.9 to 1.1. Combining the minimum and maximum values in the ideal gas equation and calculating the pressure results in estimated bounds of uncertainty from 60% to 165% of the nominal prediction. Figure 37 and Figure 38 show the pressure calculations with these additional uncertainties.

Figure 39 shows the importance factors for the response of TC18 for the conditions of TDI10-1. Before any temperature increase, the importance is associated with the environment temperature because of its connection to the component through convection on the back side. When a temperature response occurs, the activation energy becomes important initially and then is overtaken by the effective conductivity of the foam. The TC18 importance factors for the 45 lb/ft^3 foam are not included because the TC18 response is so small for the test that only the environment temperature importance stays near unity for the duration of the test. At the end of the test, the effective conductivity importance is still very small (<0.02) but begins to rise.

Figure 40 and Figure 41 are the predicted responses for TC18 presented with uncertainty for the 10 lb/ft^3 and 45 lb/ft^3 foam cases. The modeling of the TDI10-1 TC18 response is in almost exact agreement. The magnitude of the temperature response in the TDI45-1 case is much smaller than uncertainty.

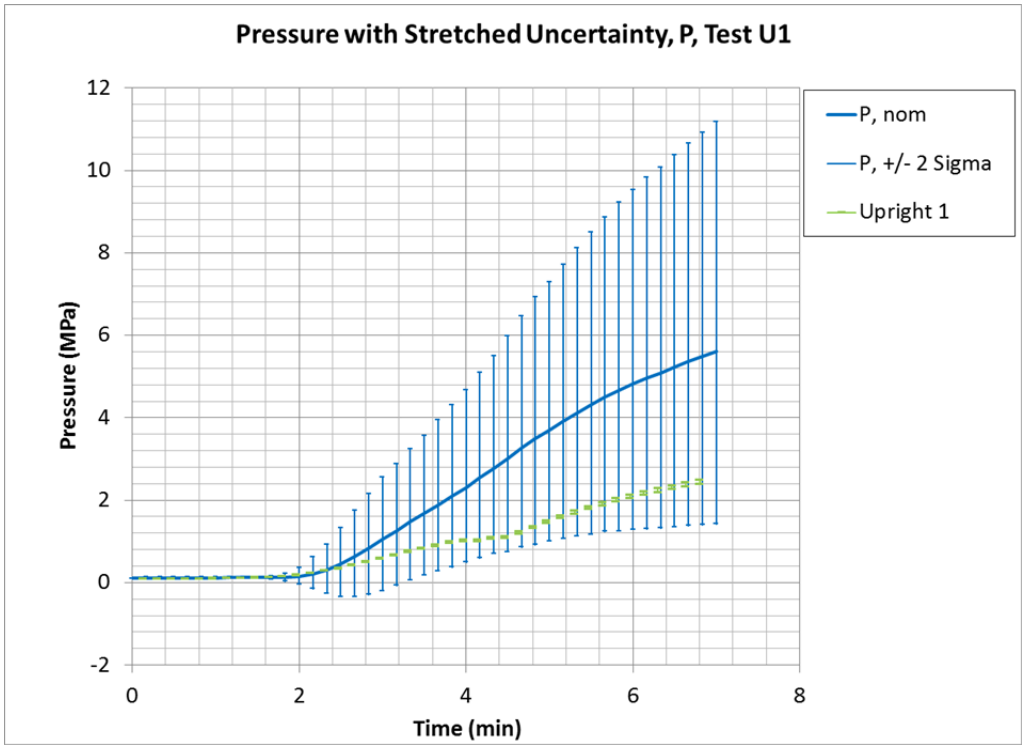

Figure 37: Model results with additional uncertainties and measured pressure for TDI45-1.

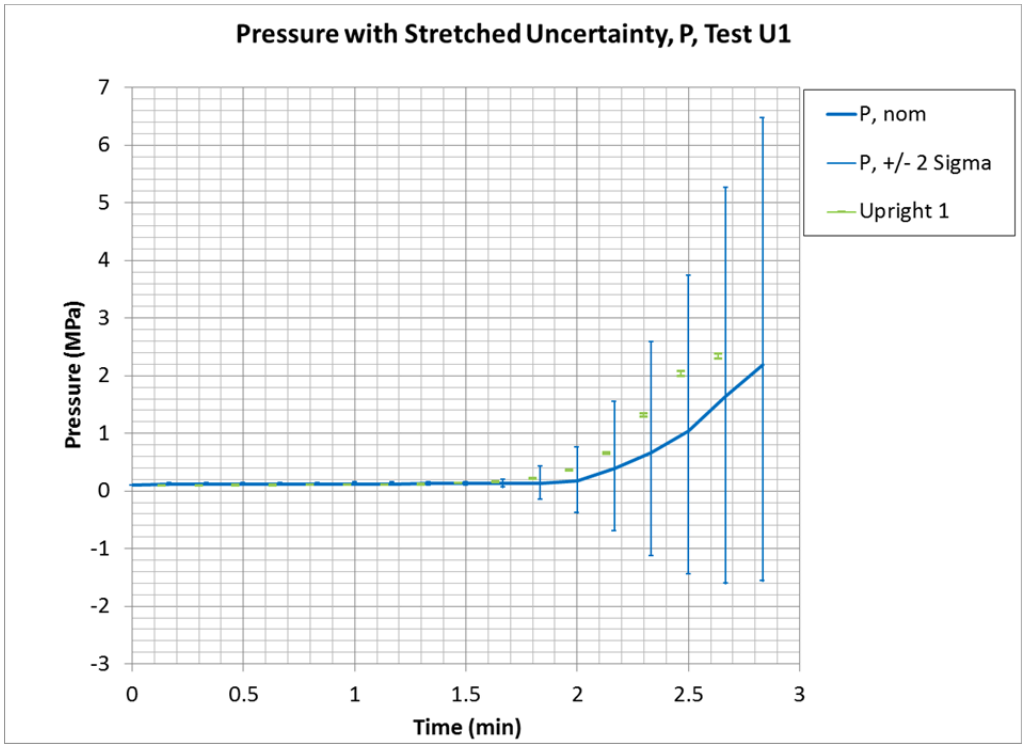

Figure 38: Model results with additional uncertainties and measured pressure for TDI45-1.

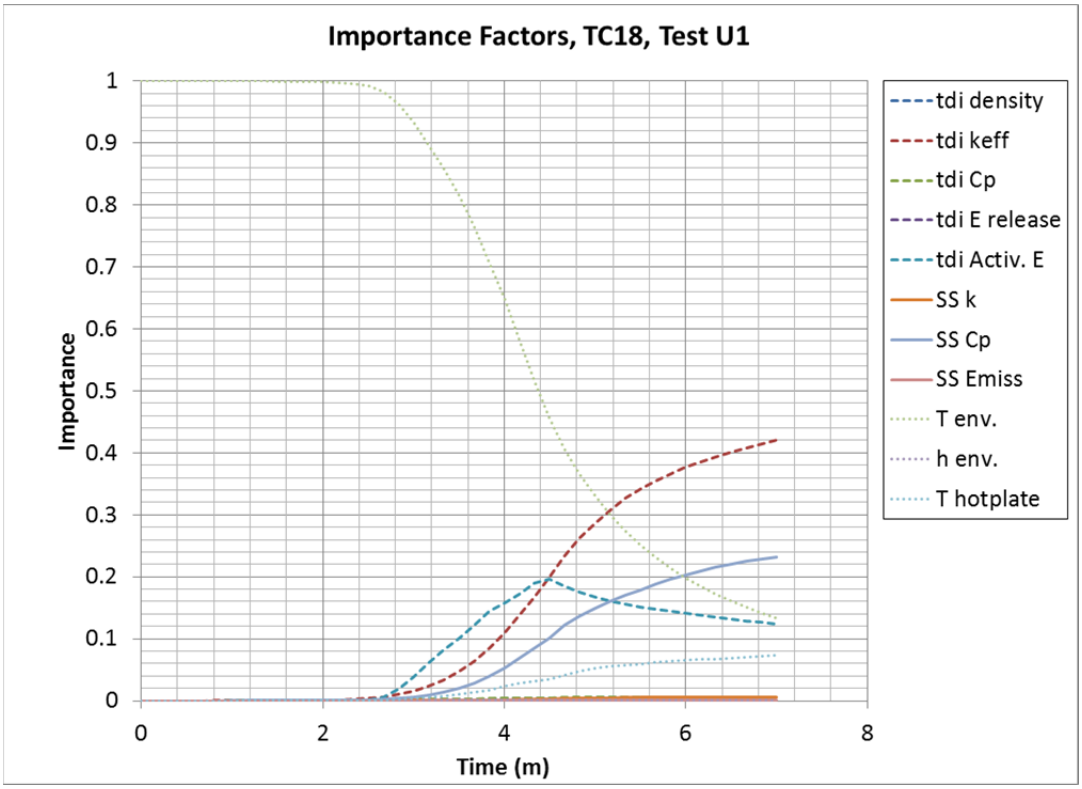

Figure 39: Importance factors for TC18 for TDI10-1.

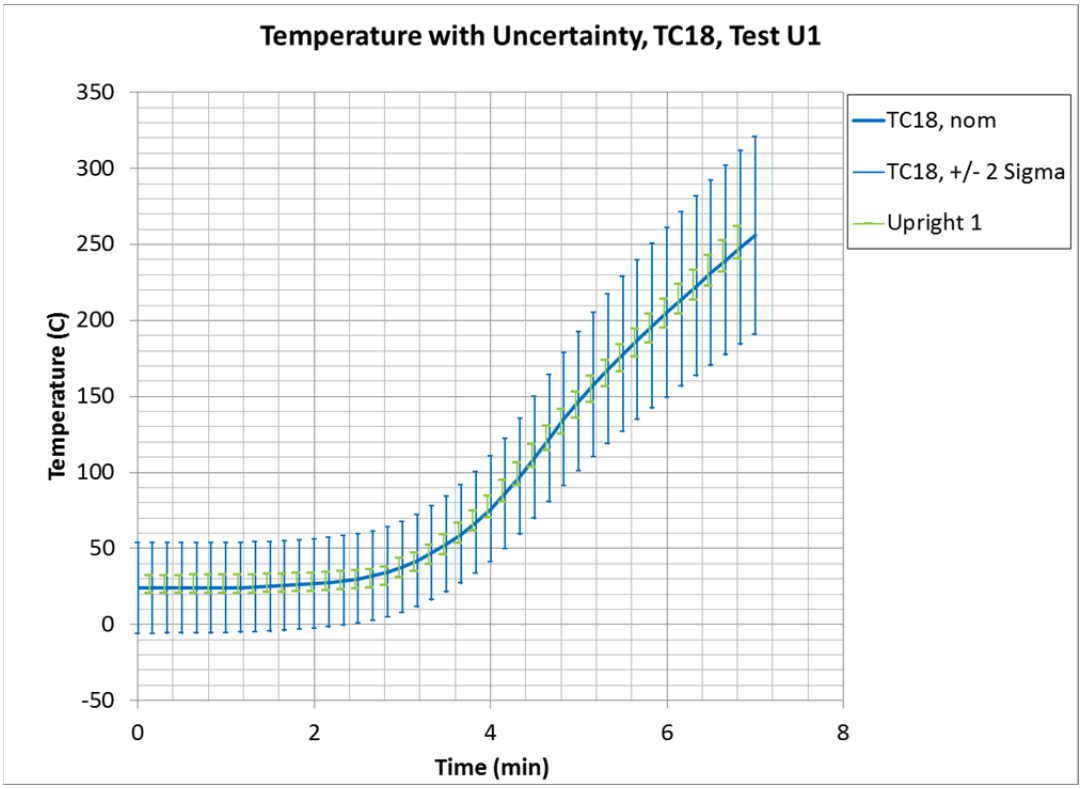

Figure 40: Modeled TC18 with uncertainty and measurements for TDI10-1.

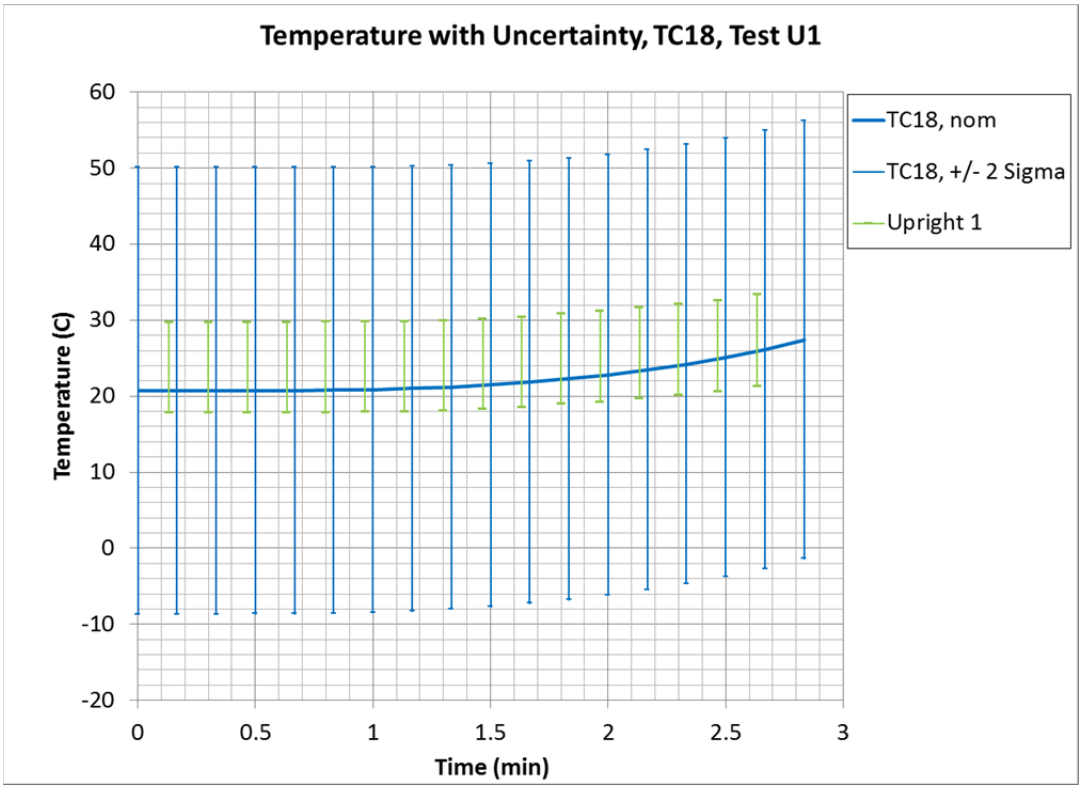

Figure 41: Modeled TC18 with uncertainty and measurements for TDI45-1.

Table 7 through Table 10 show the computed response-weighted importance factors (Eq. 13) for the four nominal densities. Each of these tables has the considered responses for Upright 1, Upright 2, Inverted 1, and Inverted 2 orientations (refer to Table 1 for details) with each row corresponding to a response and each column corresponding to a parameter.

- On each row the cell with the largest value is shaded. In no case is C_{TDI}, E_{REL}, C_{SS}, ϵ_{SS}, or h_{∞} the parameter with the greatest weighted average.
- TC2 always elects T_{hot}, this response is of little practical interest to the model because the PID controller boundary condition works to set this temperature, so TC2 can really only be influenced by uncertainty in that PID algorithm.
- k_{eff} is nearly always the most important parameter for the component response (TC17, TC18, TC20), followed by C_{SS}, however for higher densities T_{∞} becomes the most important parameter because the temperature response of the component is very small.
- k_{SS} is always the most important parameter for TC5 and is also the most important for TC6 for the lighter foams.
- TC7 and TC6 for the cases with denser foam always select T_{∞} as the most important parameter.
- TC14, at all densities, selects T_{∞} as the most important parameter.
- For the pressure response, E_{TDI}, was the most important parameter followed by $,\rho_{TDI,}C_{\mathrm{TDI}}$, and k_{eff}

The importance parameters in Table 7 through Table 10 are consistent generally consistent with expectations.

Table 7: Response-weighted Importance Factors for 10 lb/ft^3 TDI foam.

	Response	ρ_{TDI}	k_{eff}	C_{TDI}	E_{REL}	E_{TDI}	k_{SS}	C_{SS}	ϵ_{SS}	T_∞	h_∞	T_{hot}
Upright 1	TC2	0.001	0.001	0.001	0.000	0.005	0.002	0.003	0.000	0.001	0.000	0.747
	TC5	0.013	0.106	0.014	0.000	0.014	0.145	0.018	0.098	0.044	0.125	0.104
	TC6	0.016	0.069	0.018	0.000	0.025	0.149	0.019	0.049	0.092	0.110	0.034
	TC7	0.007	0.029	0.008	0.000	0.014	0.100	0.035	0.012	0.199	0.042	0.010
	TC14	0.001	0.014	0.001	0.000	0.006	0.042	0.052	0.001	0.141	0.004	0.003
	TC17	0.002	0.174	0.002	0.000	0.051	0.006	0.078	0.000	0.059	0.000	0.031
	TC18	0.002	0.159	0.002	0.000	0.048	0.002	0.085	0.000	0.062	0.000	0.028
	TC20	0.002	0.175	0.002	0.000	0.051	0.006	0.078	0.000	0.059	0.000	0.031
	P	0.074	0.029	0.016	0.000	0.300	0.006	0.005	0.002	0.015	0.003	0.009
Upright 2	TC2	0.002	0.002	0.002	0.000	0.002	0.002	0.002	0.000	0.002	0.000	0.748
	TC5	0.013	0.108	0.014	0.000	0.013	0.144	0.019	0.100	0.043	0.123	0.106
	TC6	0.016	0.072	0.018	0.000	0.024	0.148	0.020	0.050	0.091	0.110	0.035
	TC7	0.007	0.030	0.008	0.000	0.013	0.100	0.036	0.012	0.196	0.042	0.010
	TC14	0.001	0.014	0.002	0.000	0.006	0.043	0.053	0.001	0.139	0.004	0.003
	TC17	0.002	0.177	0.002	0.000	0.049	0.006	0.079	0.000	0.058	0.000	0.032
	TC18	0.002	0.162	0.002	0.000	0.046	0.002	0.086	0.000	0.061	0.000	0.029
	TC20	0.002	0.178	0.002	0.000	0.049	0.006	0.079	0.000	0.058	0.000	0.032
	P	0.076	0.030	0.015	0.000	0.299	0.007	0.005	0.002	0.015	0.003	0.009
Inverted 1	TC2	0.001	0.000	0.001	0.000	0.000	0.002	0.002	0.000	0.002	0.001	0.792
	TC5	0.013	0.073	0.014	0.000	0.023	0.166	0.018	0.070	0.061	0.149	0.106
	TC6	0.014	0.040	0.016	0.000	0.036	0.164	0.017	0.034	0.124	0.121	0.032
	TC7	0.006	0.016	0.006	0.000	0.015	0.094	0.026	0.008	0.257	0.043	0.009
	TC14	0.001	0.008	0.001	0.000	0.007	0.034	0.036	0.000	0.187	0.004	0.002
	TC17	0.002	0.134	0.002	0.000	0.089	0.004	0.058	0.000	0.091	0.000	0.026
	TC18	0.002	0.122	0.002	0.000	0.083	0.002	0.063	0.000	0.095	0.000	0.024
	TC20	0.002	0.134	0.002	0.000	0.090	0.004	0.058	0.000	0.090	0.000	0.026
	P	0.063	0.018	0.012	0.000	0.357	0.006	0.002	0.001	0.014	0.003	0.009
Inverted 2	TC2	0.000	0.000	0.000	0.000	0.000	0.001	0.002	0.000	0.001	0.000	0.801
	TC5	0.013	0.081	0.014	0.000	0.019	0.163	0.018	0.079	0.059	0.148	0.108
	TC6	0.014	0.046	0.016	0.000	0.035	0.162	0.018	0.038	0.122	0.121	0.033
	TC7	0.006	0.019	0.006	0.000	0.015	0.095	0.028	0.009	0.251	0.043	0.009
	TC14	0.001	0.010	0.001	0.000	0.007	0.036	0.040	0.001	0.181	0.004	0.002
	TC17	0.002	0.145	0.002	0.000	0.082	0.005	0.064	0.000	0.087	0.000	0.027
	TC18	0.002	0.133	0.002	0.000	0.076	0.002	0.069	0.000	0.092	0.000	0.025
	TC20	0.002	0.145	0.002	0.000	0.082	0.005	0.064	0.000	0.087	0.000	0.027
	P	0.067	0.019	0.012	0.000	0.355	0.005	0.003	0.001	0.014	0.003	0.009

Table 8: Response-weighted Importance Factors for 20 lb/ft^3 TDI foam.

	Response	ρ_{TDI}	k_{eff}	C_{TDI}	E_{REL}	E_{TDI}	k_{SS}	C_{SS}	ϵ_{SS}	T_∞	h_∞	T_{hot}
Upright 1	TC2	0.002	0.001	0.001	0.000	0.001	0.002	0.002	0.001	0.001	0.001	0.753
	TC5	0.030	0.093	0.032	0.000	0.009	0.162	0.015	0.073	0.049	0.100	0.089
	TC6	0.030	0.046	0.033	0.000	0.022	0.165	0.014	0.032	0.100	0.080	0.025
	TC7	0.011	0.017	0.012	0.000	0.009	0.100	0.025	0.008	0.213	0.031	0.007
	TC14	0.002	0.009	0.002	0.000	0.004	0.036	0.040	0.000	0.156	0.003	0.002
	TC17	0.004	0.167	0.005	0.000	0.051	0.006	0.065	0.000	0.063	0.000	0.028
	TC18	0.004	0.153	0.004	0.000	0.048	0.002	0.072	0.000	0.068	0.000	0.026
	TC20	0.004	0.168	0.005	0.000	0.051	0.006	0.065	0.000	0.063	0.000	0.029
	P	0.073	0.033	0.026	0.000	0.264	0.006	0.003	0.001	0.017	0.002	0.008
Upright 2	TC2	0.001	0.001	0.001	0.001	0.001	0.001	0.001	0.001	0.002	0.001	0.754
	TC5	0.030	0.097	0.033	0.000	0.009	0.162	0.015	0.074	0.046	0.100	0.090
	TC6	0.031	0.049	0.034	0.000	0.022	0.166	0.014	0.032	0.094	0.080	0.026
	TC7	0.012	0.018	0.013	0.000	0.010	0.103	0.026	0.008	0.205	0.031	0.007
	TC14	0.002	0.010	0.002	0.000	0.005	0.038	0.043	0.000	0.150	0.003	0.002
	TC17	0.004	0.172	0.005	0.000	0.050	0.005	0.068	0.000	0.059	0.000	0.029
	TC18	0.004	0.158	0.004	0.000	0.046	0.002	0.075	0.000	0.063	0.000	0.027
	TC20	0.004	0.172	0.005	0.000	0.050	0.005	0.068	0.000	0.059	0.000	0.029
	P	0.074	0.035	0.027	0.000	0.261	0.006	0.003	0.001	0.017	0.002	0.008
Inverted 1	TC2	0.001	0.000	0.001	0.000	0.000	0.002	0.002	0.000	0.002	0.000	0.811
	TC5	0.026	0.053	0.028	0.000	0.040	0.191	0.015	0.048	0.072	0.124	0.090
	TC6	0.023	0.021	0.025	0.000	0.031	0.185	0.013	0.022	0.149	0.096	0.024
	TC7	0.008	0.008	0.008	0.000	0.011	0.089	0.017	0.005	0.292	0.032	0.006
	TC14	0.001	0.005	0.001	0.000	0.006	0.027	0.025	0.000	0.213	0.003	0.002
	TC17	0.004	0.118	0.004	0.000	0.102	0.004	0.044	0.000	0.109	0.000	0.022
	TC18	0.003	0.109	0.004	0.000	0.094	0.002	0.048	0.000	0.117	0.000	0.021
	TC20	0.004	0.118	0.004	0.000	0.103	0.004	0.044	0.000	0.109	0.000	0.022
	P	0.063	0.018	0.016	0.000	0.348	0.005	0.001	0.001	0.015	0.002	0.007
Inverted 2	TC2	0.001	0.000	0.002	0.000	0.000	0.001	0.003	0.000	0.001	0.000	0.805
	TC5	0.026	0.062	0.028	0.000	0.030	0.184	0.015	0.055	0.067	0.126	0.093
	TC6	0.024	0.027	0.026	0.000	0.031	0.180	0.013	0.025	0.138	0.097	0.026
	TC7	0.008	0.010	0.009	0.000	0.011	0.092	0.019	0.006	0.276	0.033	0.006
	TC14	0.001	0.006	0.002	0.000	0.006	0.030	0.029	0.000	0.202	0.003	0.002
	TC17	0.004	0.128	0.004	0.000	0.095	0.004	0.049	0.000	0.100	0.000	0.024
	TC18	0.003	0.118	0.004	0.000	0.088	0.002	0.054	0.000	0.106	0.000	0.022
	TC20	0.004	0.128	0.004	0.000	0.096	0.004	0.049	0.000	0.099	0.000	0.024
	P	0.063	0.021	0.019	0.000	0.340	0.005	0.002	0.001	0.016	0.002	0.008

Table 9: Response-weighted Importance Factors for 30 lb/ft^3 TDI foam.

	Response	ρ_{TDI}	k_{eff}	C_{TDI}	E_{REL}	E_{TDI}	k_{SS}	C_{SS}	ϵ_{SS}	T_∞	h_∞	T_{hot}
Upright 1	TC2	0.001	0.001	0.001	0.000	0.001	0.001	0.001	0.000	0.001	0.001	0.786
	TC5	0.041	0.065	0.045	0.000	0.017	0.190	0.013	0.048	0.059	0.095	0.079
	TC6	0.034	0.022	0.037	0.000	0.020	0.188	0.011	0.020	0.122	0.073	0.020
	TC7	0.012	0.008	0.012	0.000	0.008	0.097	0.018	0.005	0.249	0.026	0.005
	TC14	0.002	0.006	0.002	0.000	0.005	0.030	0.029	0.000	0.184	0.002	0.002
	TC17	0.006	0.146	0.007	0.000	0.072	0.005	0.051	0.000	0.080	0.000	0.025
	TC18	0.005	0.136	0.006	0.000	0.067	0.002	0.057	0.000	0.086	0.000	0.023
	TC20	0.006	0.147	0.007	0.000	0.072	0.005	0.051	0.000	0.080	0.000	0.025
	P	0.091	0.027	0.025	0.000	0.271	0.005	0.002	0.001	0.017	0.001	0.008
Upright 2	TC2	0.001	0.001	0.001	0.000	0.001	0.002	0.005	0.000	0.002	0.001	0.780
	TC5	0.043	0.081	0.047	0.000	0.009	0.180	0.013	0.058	0.052	0.089	0.079
	TC6	0.038	0.031	0.041	0.000	0.018	0.182	0.012	0.024	0.107	0.069	0.021
	TC7	0.013	0.011	0.014	0.000	0.007	0.101	0.021	0.006	0.226	0.026	0.006
	TC14	0.002	0.008	0.003	0.000	0.004	0.034	0.035	0.000	0.167	0.002	0.002
	TC17	0.007	0.166	0.007	0.000	0.055	0.005	0.059	0.000	0.067	0.000	0.028
	TC18	0.006	0.154	0.006	0.000	0.051	0.003	0.066	0.000	0.073	0.000	0.026
	TC20	0.007	0.167	0.007	0.000	0.055	0.005	0.059	0.000	0.067	0.000	0.028
	P	0.097	0.033	0.029	0.000	0.249	0.006	0.002	0.001	0.018	0.002	0.007
Inverted 1	TC2	0.000	0.000	0.000	0.000	0.000	0.002	0.003	0.000	0.001	0.000	0.833
	TC5	0.029	0.020	0.031	0.000	0.073	0.215	0.012	0.026	0.104	0.111	0.078
	TC6	0.022	0.006	0.023	0.000	0.025	0.188	0.009	0.012	0.216	0.084	0.020
	TC7	0.006	0.002	0.007	0.000	0.007	0.070	0.009	0.002	0.363	0.023	0.004
	TC14	0.001	0.002	0.001	0.000	0.004	0.017	0.012	0.000	0.258	0.002	0.001
	TC17	0.004	0.078	0.005	0.000	0.114	0.002	0.026	0.000	0.168	0.000	0.014
	TC18	0.004	0.073	0.004	0.000	0.103	0.001	0.028	0.000	0.177	0.000	0.013
	TC20	0.004	0.079	0.005	0.000	0.115	0.002	0.026	0.000	0.167	0.000	0.014
	P	0.051	0.009	0.011	0.000	0.403	0.002	0.000	0.000	0.011	0.001	0.006
Inverted 2	TC2	0.001	0.001	0.001	0.000	0.000	0.001	0.002	0.000	0.001	0.000	0.835
	TC5	0.029	0.023	0.032	0.000	0.072	0.214	0.011	0.028	0.099	0.112	0.079
	TC6	0.022	0.007	0.024	0.000	0.026	0.190	0.009	0.013	0.208	0.084	0.020
	TC7	0.007	0.002	0.007	0.000	0.008	0.072	0.010	0.003	0.356	0.024	0.004
	TC14	0.001	0.002	0.001	0.000	0.004	0.018	0.013	0.000	0.254	0.002	0.001
	TC17	0.005	0.083	0.005	0.000	0.115	0.002	0.027	0.000	0.161	0.000	0.015
	TC18	0.004	0.077	0.004	0.000	0.104	0.001	0.030	0.000	0.171	0.000	0.014
	TC20	0.005	0.083	0.005	0.000	0.115	0.002	0.027	0.000	0.161	0.000	0.015
	P	0.055	0.011	0.011	0.000	0.398	0.002	0.000	0.000	0.011	0.001	0.007

Table 10: Response-weighted Importance Factors for 45 lb/ft^3 TDI foam.

	Response	ρ_{TDI}	k_{eff}	C_{TDI}	E_{REL}	E_{TDI}	k_{SS}	C_{SS}	ϵ_{SS}	T_∞	h_∞	T_{hot}
Upright 1	TC2	0.002	0.002	0.002	0.000	0.000	0.001	0.003	0.000	0.001	0.000	0.843
	TC5	0.034	0.009	0.037	0.000	0.063	0.238	0.009	0.017	0.129	0.098	0.068
	TC6	0.023	0.002	0.024	0.000	0.016	0.184	0.006	0.007	0.259	0.066	0.015
	TC7	0.006	0.001	0.006	0.000	0.004	0.058	0.006	0.001	0.391	0.016	0.003
	TC14	0.001	0.001	0.001	0.000	0.003	0.012	0.007	0.000	0.273	0.001	0.001
	TC17	0.005	0.064	0.006	0.000	0.106	0.002	0.018	0.000	0.201	0.000	0.011
	TC18	0.005	0.059	0.005	0.000	0.097	0.001	0.019	0.000	0.210	0.000	0.010
	TC20	0.005	0.064	0.006	0.000	0.106	0.002	0.018	0.000	0.201	0.000	0.011
	P	0.054	0.005	0.007	0.000	0.415	0.001	0.000	0.000	0.008	0.000	0.006
Upright 2	TC2	0.000	0.000	0.000	0.000	0.000	0.002	0.001	0.000	0.001	0.000	0.851
	TC5	0.034	0.009	0.037	0.000	0.064	0.238	0.009	0.017	0.129	0.099	0.068
	TC6	0.023	0.002	0.024	0.000	0.016	0.185	0.006	0.007	0.258	0.067	0.015
	TC7	0.006	0.001	0.006	0.000	0.004	0.058	0.006	0.001	0.391	0.016	0.003
	TC14	0.001	0.001	0.001	0.000	0.003	0.012	0.008	0.000	0.273	0.001	0.001
	TC17	0.005	0.065	0.006	0.000	0.106	0.002	0.018	0.000	0.200	0.000	0.011
	TC18	0.005	0.060	0.005	0.000	0.098	0.001	0.020	0.000	0.209	0.000	0.010
	TC20	0.006	0.065	0.006	0.000	0.107	0.002	0.018	0.000	0.199	0.000	0.011
	P	0.057	0.005	0.007	0.000	0.415	0.001	0.000	0.000	0.007	0.000	0.006
Inverted 1	TC2	0.000	0.000	0.000	0.000	0.000	0.002	0.003	0.000	0.002	0.000	0.863
	TC5	0.029	0.004	0.030	0.000	0.045	0.245	0.009	0.013	0.176	0.106	0.067
	TC6	0.018	0.002	0.019	0.000	0.010	0.166	0.005	0.005	0.322	0.064	0.013
	TC7	0.004	0.000	0.004	0.000	0.002	0.046	0.004	0.001	0.435	0.014	0.002
	TC14	0.001	0.001	0.001	0.000	0.001	0.009	0.005	0.000	0.297	0.001	0.000
	TC17	0.004	0.043	0.004	0.000	0.086	0.001	0.012	0.000	0.264	0.000	0.007
	TC18	0.003	0.039	0.004	0.000	0.080	0.001	0.013	0.000	0.270	0.000	0.007
	TC20	0.004	0.043	0.004	0.000	0.087	0.001	0.012	0.000	0.263	0.000	0.007
	P	0.023	0.002	0.003	0.000	0.452	0.001	0.000	0.000	0.004	0.000	0.006
Inverted 2	TC2	0.001	0.002	0.001	0.000	0.000	0.003	0.002	0.000	0.003	0.002	0.857
	TC5	0.030	0.005	0.031	0.000	0.053	0.241	0.009	0.014	0.168	0.104	0.068
	TC6	0.019	0.002	0.019	0.000	0.012	0.168	0.005	0.006	0.313	0.064	0.014
	TC7	0.005	0.000	0.005	0.000	0.003	0.047	0.004	0.001	0.429	0.014	0.002
	TC14	0.001	0.001	0.001	0.000	0.002	0.009	0.005	0.000	0.293	0.001	0.000
	TC17	0.004	0.046	0.004	0.000	0.095	0.001	0.013	0.000	0.250	0.000	0.008
	TC18	0.004	0.042	0.004	0.000	0.087	0.001	0.014	0.000	0.257	0.000	0.007
	TC20	0.004	0.046	0.005	0.000	0.096	0.001	0.013	0.000	0.250	0.000	0.008
	P	0.028	0.003	0.004	0.000	0.453	0.001	0.000	0.000	0.005	0.000	0.006

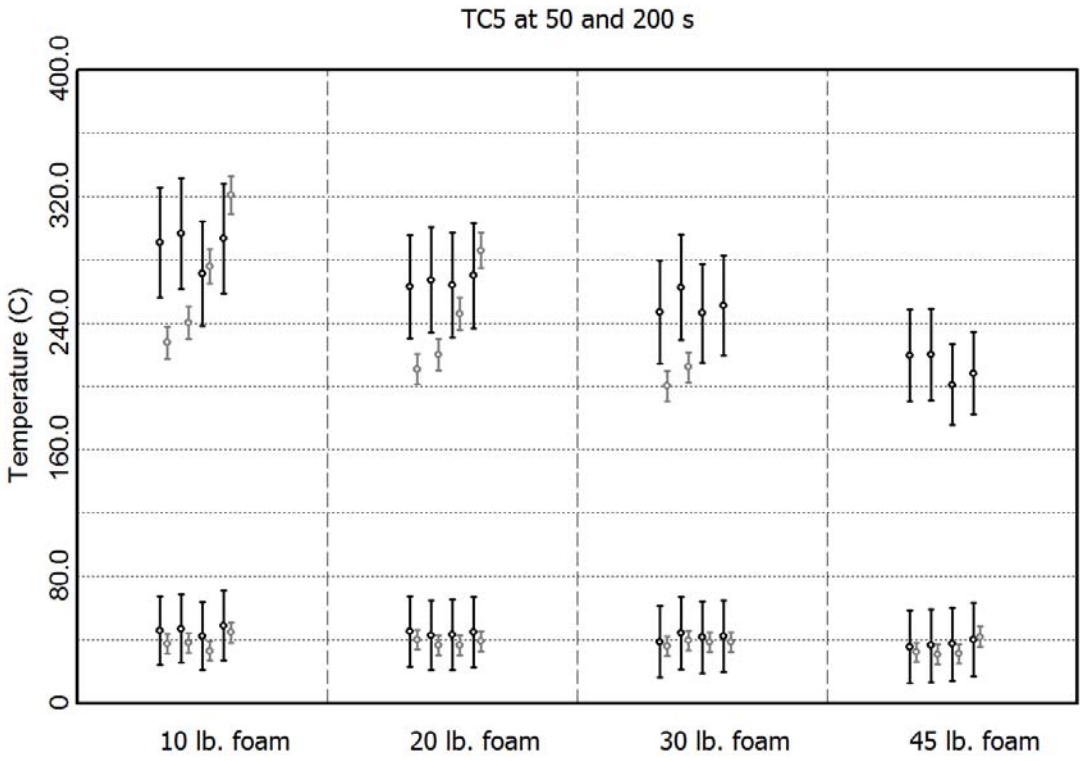

Figure 42: TC5 model predictions with uncertainty and measurements for all test conditions for time 50 and 200s.

Figure 42 through Figure 47 show model predictions with uncertainty along with measurements at selected times for TC5, TC6, TC7, TC14, TC17 and Pressure. In each of these plots available results for all sixteen tests are represented. (In some cases the test data were not available at the specified times.) In each plot, the black symbol collection represents the prediction and the gray symbol collection the measurement. As labeled along the bottom, the four vertical panels correspond to the four nominal densities. In each of these panels, four sets of the symbols from left to right correspond to Upright 1, Upright 2, Inverted 1, and Inverted 2 tests. Depending upon how the data fit within this framework, one or two times were considered. If two different times are indicated, the higher set of symbols always belongs to the latter time as all the variables increase monotonically.

Figure 42 shows a composite of results for all of the tests for the TC5 location. At 50s all system had a response in the vicinity of 40°C and model effectively captures the data. This precedes foam decomposition and the model is dominated by conduction so it is not a surprise that the agreement is satisfactory.

At 200s (not available for all test measurements) more interesting dynamics have occurred and the model does not capture the data.

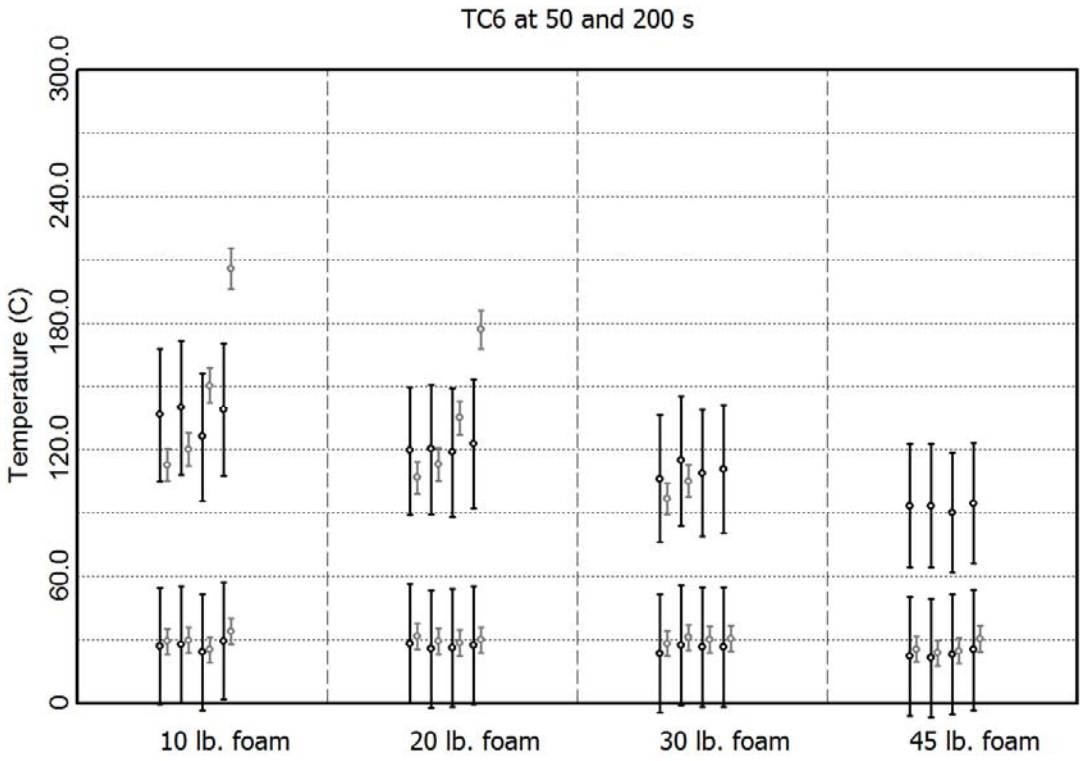

Figure 43: TC6 model predictions with uncertainty and measurements for all test conditions for time 50 and 200s.

Figure 43 corresponds to times of 50 and 200s for TC6. At the early time, the response is due to conduction and the model succeeds convincingly. As noted in Section 3, events (likely gaseous tunneling) occur in the experiment and the measurements have sharp increases in temperatures at later times that are stochastic in nature and that the model does not describe.

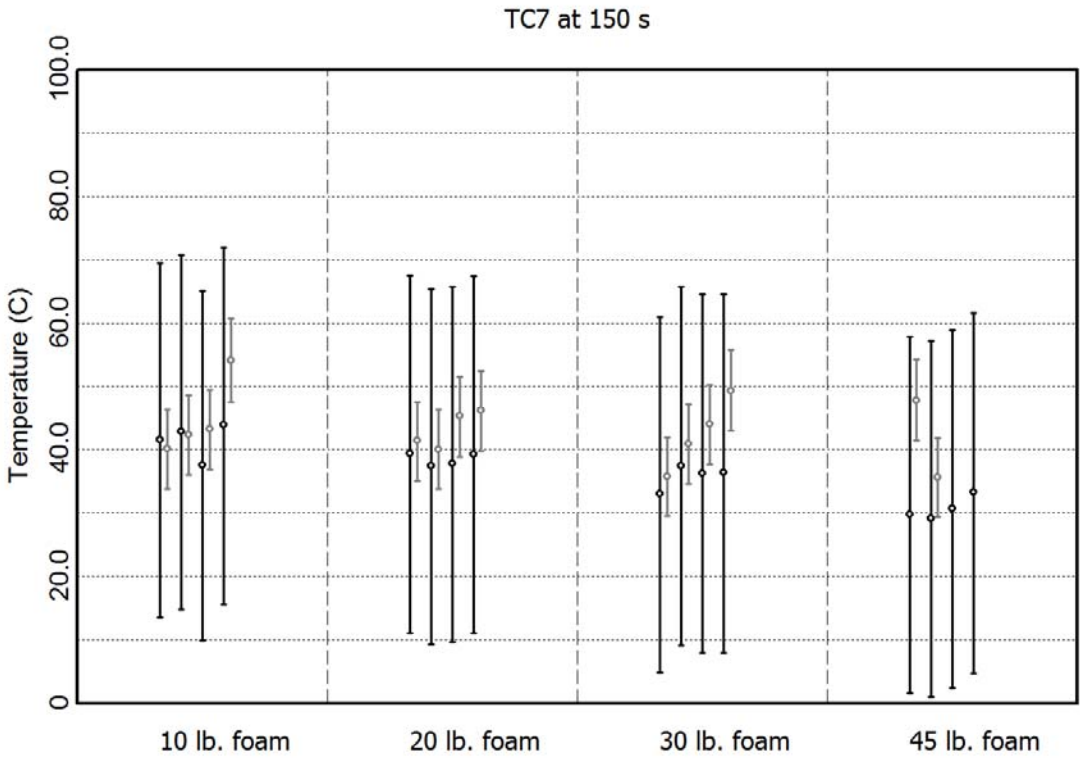

Figure 44: TC7 model predictions with uncertainty and measurements for all test conditions for time 150s.

Figure 44 shows experimental results for the 14 tests of duration of at least 150s for the TC7 location. The model uncertainty intervals encompass the available experimental data. This location is far enough from the heated surface that transient conduction in the stainless steel is more important to the response than the foam-characterizing parameters.

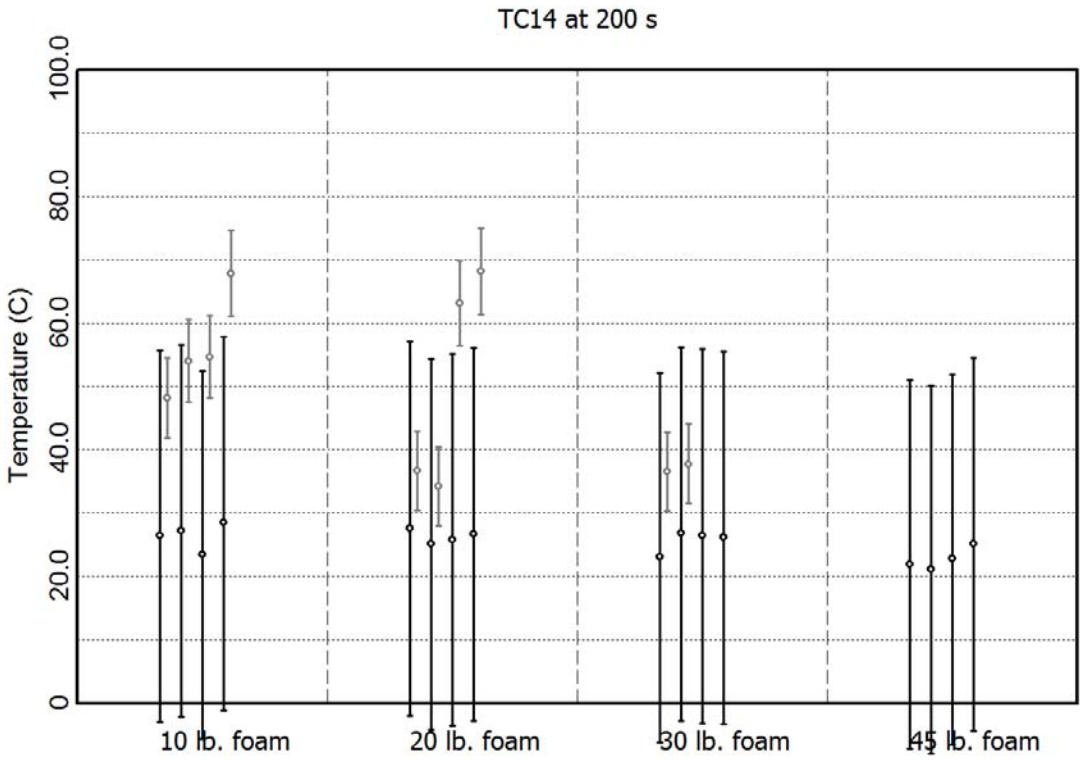

Figure 45: TC14 model predictions with uncertainty and measurements for all test conditions for time 200s.

Figure 45 shows the TC14 location, which is located farthest from the heated boundary of the can. The nominal predictions all under predict the nominal measurements indicating that the convective contribution may be overestimated in the model or the foam may be too insulating. However, as noted in the results section, it appeared that gas tunneling had the influence of suddenly heating areas past the front of thermal conduction response, which could be showing up in the experimental response of TC14. Figure 45 illustrates a condition for which there appears to be clear separation between the responses of the two experimental orientations.

Figure 46 shows the comparison for TC17, which is near the component face. The model uncertainty intervals bound the measured data.

Figure 47 show predicted and measured pressures along with uncertainties. The uncertainty intervals for the pressure calculation are only those associated with the mean value method propagating uncertainty of the parameters in Table 5 and do not include the model form error multipliers that were previously discussed. As demonstrated earlier (Figure 35), the measurements fall outside of the predictions, however, if the additional model form error is included, they would fall within the error bounds.

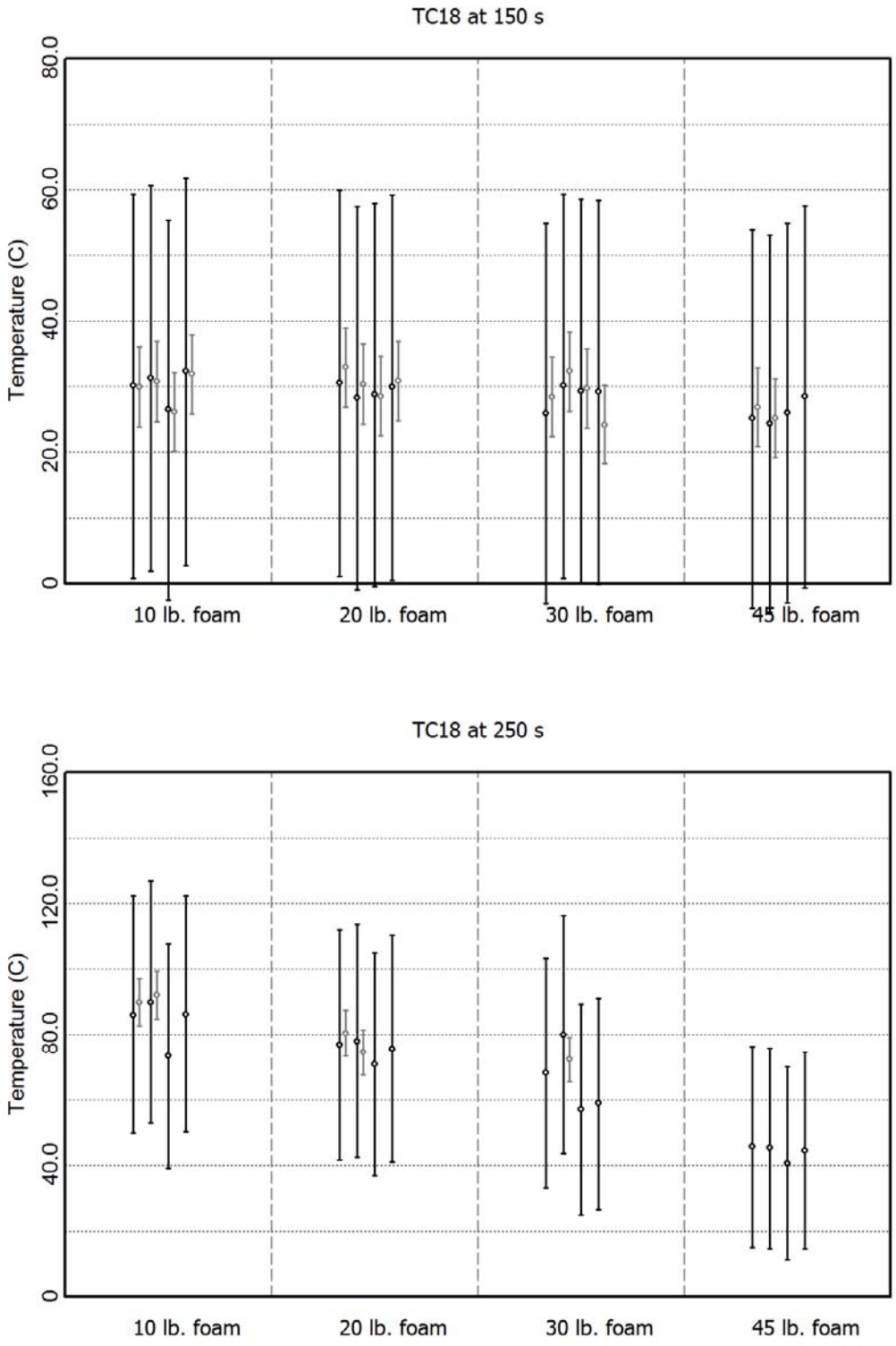

Figure 46: TC17 model predictions with uncertainty and measurements for all test conditions for time 150 and 250s.

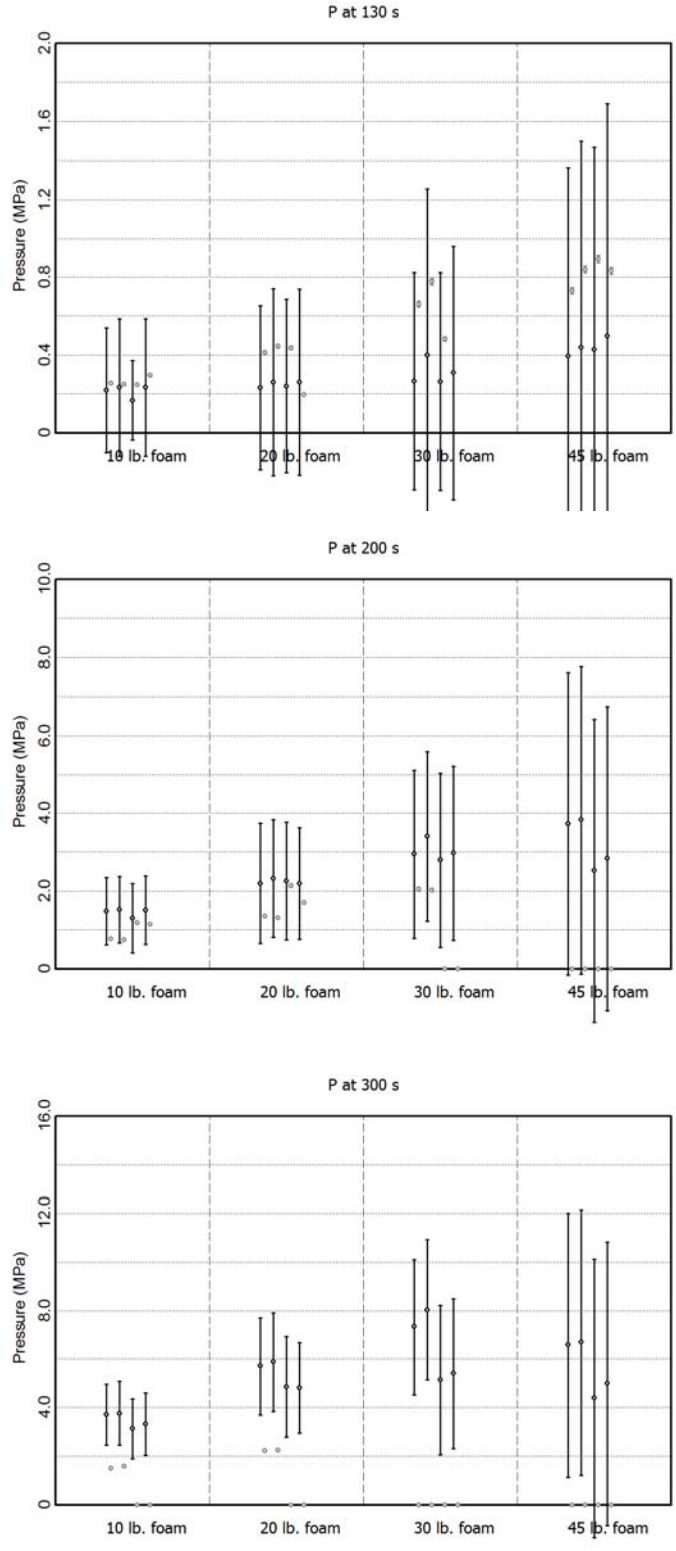

Figure 47: Pressure model predictions with uncertainty and measurements for all test conditions for time 130, 200, and 300s.

Linearity of Model

Estimation of the propagated uncertainty according to Eq. 8 assumes a linear model response over the range of the parameter uncertainty. As noted earlier the sensitivity estimates used in Eq. 8 were based on central difference operators (Eq. 6). Sensitivities were also calculated at each response location and time based on forward and backward differences in the parameter. These results were inspected to establish model linearity. By definition the central difference estimate is the average of the forward and backward estimate. So if two of the estimates are in agreement, all three are in agreement (the defect in agreement between the backward and central difference must be opposite and equal that between the forward and central difference). Consequently, the difference between backward difference estimates are compared to center difference results (and the comparison with forward is known be complementary).

To conduct the comparison, for each response at each density:

- The earliest time step at which the predicted response increase was half of the increase at the end of the analysis was identified. (For pressure the time at which half of the maximum allowed pressure (2.5MPa) was identified.)
- At the time identified in the previous step the central-difference sensitivities of the response with respect of each of the study parameters was examined and the maximum sensitivity $\left|\frac{\partial R_j}{\partial P_i}\right|_{max}$ was saved as a scaling factor.
- The differences between the sensitivity for backward and central differencing were calculated and scaled by the maximum sensitivity identified in the previous step, i.e,

$$\Delta\frac{\partial R_j}{\partial P_i}^{*} = \left\{\left(\frac{\partial R_j}{\partial P_i}\right)_{backward} - \left(\frac{\partial R_j}{\partial P_i}\right)_{central}\right\} \Big/ \left|\frac{\partial R_j}{\partial P_i}\right|_{max} \qquad (14)$$

The following table reports differences in sensitivity estimates, as defined by $\Delta\frac{\partial R_j}{\partial P_i}^{*}$, for each response and each density. The RMS difference is calculated for the 11 different parameters that were used in the study. The maximum difference in the comparison is also given and the associated parameter identified in the last column. The most significant departures from linearity by this measure are associated with the pressure response and the worst of those are associated with activation energy and the two densest foams. Aside from the pressure estimate the backward differencing estimates are generally within about 1% of the central difference estimate.

The results of the table demonstrate that the model response is sufficiently linear to allow the mean value method to provide reasonable estimates of uncertainty.

Table 11: Summary comparison of backward and central differences for all responses

Density	Response	RMS (%)	Max. (%)		Parameter	Response	RMS (%)	Max. (%)	Parameter
10	P	3.1	8.0		T_{hot}	TC14	0.90	2.9	T_{∞}
20	P	1.5	3.3		T_{hot}	TC14	0.77	2.4	T_{∞}
30	P	3.3	10		E_{TDI}	TC14	0.62	1.8	T_{∞}
45	P	7.1	21		E_{TDI}	TC14	0.27	0.68	T_{∞}
10	TC5	1.3	3.6		T_{hot}	TC17	0.73	2.0	T_{hot}
20	TC5	0.96	2.7		T_{hot}	TC17	0.77	2.2	T_{hot}
30	TC5	0.66	1.5		T_{hot}	TC17	1.21	3.5	T_{hot}
45	TC5	1.0	3.0		T_{hot}	TC17	0.75	2.1	T_{∞}
10	TC6	0.68	2.0		T_{hot}	TC18	0.75	2.0	T_{hot}
20	TC6	0.94	2.2		T_{hot}	TC18	0.79	2.2	T_{hot}
30	TC6	0.80	2.1		T_{hot}	TC18	1.2	3.3	T_{hot}
45	TC6	0.61	1.3		T_{∞}	TC18	0.68	1.7	T_{∞}
10	TC7	0.57	1.5		T_{∞}	TC20	0.74	2.0	T_{hot}
20	TC7	0.46	1.0		T_{∞}	TC20	0.80	2.3	T_{hot}
30	TC7	0.41	0.82		T_{∞}	TC20	1.2	3.5	T_{hot}
45	TC7	0.22	0.35		T_{∞}	TC20	0.78	2.2	T_{∞}
All Responses		1.70	21						

9. CONCLUSIONS

The mean value method was applied to estimate uncertainty intervals for temperature and pressure response estimates. The model does not include gravity and relocation of material that occurs in an orientation-dependent manner. It is very clear from this analysis that important physics are missing from the model.

Ideally, the foam in can studies would isolate the behavior of the foam so that using the same model of the foam thermo/chemical properties with another container/geometry would be certain to give reliable results. The current study considers only a very limited set of conditions. For example, all of these tests were conducted at the same heating rate and terminal boundary temperature. In future work, it would be beneficial to examine a range of heating rates, densities, multiple materials, and added free volume to gain additional insight.

The effective volume of the system containing the gases is not well known, but it appears to be consistent as transient pressure measurement between replicate tests compare very well. There is evidently enough gas flow and/or distortion of remaining closed cells during the pressure evolution to insure a consistent response. Temperature measurements exhibit sharp rises due to

the movement of hotter gaseous products. The continuum model implemented has no prospect of duplicating those behaviors which, given a very large number of observations, could only be characterized in a stochastic manner. The system under study exhibits:

- Fluctuating temperatures potentially due to local flow channeling.
- Dependence on gravity potentially due to liquefied decomposition products moving towards the heated boundary and undergoing decomposition into the gas phase when the system is inverted, while in an upright configuration, the liquefied decomposition products and reaction front is moving away from the heated surface.

If both of these phenomena were small relative to the uncertainties that arise from the model parameters they might regarded as acceptable sources of noise. The temperature fluctuations may be acceptable. The present method of model comparison would indicate model success at additional time/locations if the measurements were filtered (brief excursions discounted). The pressure exhibits clear dependencies on gravity which are very significant relative to the uncertainty arising from the model parameters.

The rate of energy transfer through the thin foam thickness between the component and the heated boundary appears to be well represented as the measured component responses fall well within the expected model uncertainty intervals. The data include less component response for the denser foams which resulted in shorter tests due to the faster rise to the maximum allowed pressure.

10. REFERENCES

1. Erickson, K. L., Dodd, A. B., and E. C. Quintana, "Physical Behavior and Container Pressurization During Thermal Decomposition of Polyurethane Foams," Proceedings of BCC 2011, Stamford, CT, 23-25 May 2011.
2. Erickson, K. L., Dodd, A. B., Hogan, R. E., and Dowding, K. J. "Heat Transfer, Foam Decomposition, and Container Pressurization: Comparison of Experimental and Modeling Results," Proc, of Interflam 2010, Nottingham, UK, 5-7 July 2010.
3. Erickson, K. L., Dodd, A. B., and Hogan, R. E., "Modeling Pressurization Caused by Thermal Decomposition of Highly Charring Foam in Sealed Containers," Proceedings of BCC 2010, Stamford, CT, 23-26 May 2010.
4. https://computing.sandia.gov/codes_and_tools/Aria
5. Siegel, R. and Howell, J. R., Thermal Radiation Heat Transfer, 4th ed., Taylor and Francis, New York, 2002, Appendix B.
6. Hills, R. G. and Trucano, T. G., "Statistical Validation of Engineering and Scientific Models: Background," SAND1999-1256, Sandia National Laboratories, Albuquerque, NM, May 1999.
7. Oberkampf, W.L. and C.J. Roy, Verification and Validation in Scientific Computing, Cambridge University Press, 2010.

Distribution

1 MS-0836	01514	M. Larsen
1 MS-0346	01514	D. Dobranich
1 MS-0836	01514	N. Francis
1 MS-0836	01514	R. Hogan
1 MS-0828	01514	M. Pilch
1 MS-0836	01514	J. Shelton
1 MS-0828	01544	A. Black
1 MS-0386	01544	K. Dowding
1 MS-0828	01544	R. Hills
1 MS-0812	01544	V. Romero
1 MS-9042	08365	A. Dodd
1 MS-9042	08365	S. Scott
1 MS-9957	08365	G. Wagner
1 MS-9957	08365	V.Brunini
1 MS-9957	08365	R.Keedy
1 MS-9957	08365	J. Templeton
1 MS-1135	01532	J. Suo-Anttila
1 MS-0836	01514	J. Yuan
1 MS-0836	01514	E. Silva
1 MS-0346	01526	R. Teeter


Sandia National Laboratories